Searching for $H \to hh \to b\bar{b}\tau\tau$ in the 2HDM type-I at the LHC

A. Arhrib,[1,2,*] S. Moretti,[3,4,†] S. Semlali,[3,5,‡] C. H. Shepherd-Themistocleous,[5,§] Y. Wang,[6,7,‖] and Q. S. Yan[8,9,¶]

[1]*Abdelmalek Essaadi University, Faculty of Sciences and Techniques, B.P. 2117 Tétouan, Tanger, Morocco*
[2]*Department of Physics and Center for Theory and Computation, National Tsing Hua University, Hsinchu, Taiwan 300*
[3]*School of Physics and Astronomy, University of Southampton, Southampton, SO17 1BJ, United Kingdom*
[4]*Department of Physics and Astronomy, Uppsala University, Box 516, SE-751 20 Uppsala, Sweden*
[5]*Particle Physics Department, Rutherford Appleton Laboratory, Chilton, Didcot, Oxon OX11 0QX, United Kingdom*
[6]*College of Physics and Electronic Information, Inner Mongolia Normal University, Hohhot 010022, People's Republic of China*
[7]*Inner Mongolia Key Laboratory for Physics and Chemistry of Functional Materials, Inner Mongolia Normal University, Hohhot, 010022, China*
[8]*Center for Future High Energy Physics, Chinese Academy of Sciences, Beijing 100049, People's Republic of China*
[9]*School of Physics Sciences, University of Chinese Academy of Sciences, Beijing 100039, People's Republic of China*

(Received 6 December 2023; accepted 12 February 2024; published 13 March 2024)

Unlike other realizations of the 2-Higgs doublet model (2HDM), the so-called type-I allows for a very light Higgs boson spectrum. Specifically, herein, the heaviest of the two CP-even neutral Higgs states, H, can be the one discovered at the Large Hadron Collider (LHC) in 2012, with a mass of ≈125 GeV and couplings consistent with those predicted by the Standard Model (SM). In such a condition of the model, referred to as "inverted mass hierarchy," the decay of the SM-like Higgs state into pairs of the lightest CP-even neutral Higgs boson, h, is possible, for masses of the latter ranging from $M_H/2 \approx 65$ GeV down to 15 GeV or so, all compatible with experimental constraints. In this paper, we investigate the scope of the LHC in accessing the process $gg \to H \to hh \to b\bar{b}\tau\tau$ by performing a Monte Carlo (MC) analysis aimed at extracting this signal from the SM backgrounds, in presence of a dedicated trigger choice and kinematic selection. We prove that some sensitivity to such a channel exists already at run 3 of the LHC while the High-Luminosity LHC (HL-LHC) will be able to either confirm or disprove this theoretical scenario over sizable regions of its parameter space.

DOI: 10.1103/PhysRevD.109.055020

I. INTRODUCTION

In the SM of particle physics, it is well known that the Higgs boson [1,2] is responsible for the generation of fermion and gauge boson masses through what is called spontaneous symmetry breaking (SSB) [3,4]. Such a mechanism also predicts a self-interaction for the Higgs state.

The measurement of such a self-coupling is the only experimental way to understand the SSB mechanism and to reconstruct the Higgs potential responsible for it. This is an important (and challenging) task also because it can shed some light on possible beyond the SM (BSM) effects that may affect Higgs self-couplings in general.

The LHC has started a new campaign of measurements after the recent upgrade, the so-called run 3. This will involve, among other things, measuring ever more precisely the coupling of the SM-like Higgs boson to other SM particles or even progressing toward the measurement of its self-coupling. The LHC is also capable of measuring new decays of the SM-like Higgs boson into non-SM particles.

*a.arhrib@gmail.com
†s.moretti@soton.ac.uk, stefano.moretti@physics.uu.se
‡souad.semlali@soton.ac.uk
§claire.shepherd@stfc.ac.uk
‖wangyan@imnu.edu.cn
¶yanqishu@ucas.ac.cn

Current results from the ATLAS and CMS experiments indicate that the measured SM-like Higgs signal rates in all channels agree well with the SM theoretical predictions at the $\sim 2\sigma$ level [5,6]. However, there are several pieces of evidences, both theoretical (the hierarchy problem, the absence of gauge coupling unification, etc.) and experimental (neutrino masses, the matter-antimatter asymmetry, etc.), which indicate that the SM could not be the ultimate description of Nature but should be viewed as a low-energy effective theory of some more fundamental one yet to be discovered.

There exist several BSM theories that address these weaknesses of the SM while identifying the 125 GeV scalar particle as a part of an extended scalar sector. One of the simplest extensions of the SM is the 2HDM, which contains two Higgs doublets, Φ_1 and Φ_2, which give masses to all fermions and gauge bosons. The particle spectrum of the 2HDM is as follows: two CP-even (h and H, with $m_h < m_H$, one of them being identified with the SM-like Higgs boson with mass 125 GeV: H in our case), one CP-odd (A) and a pair of charged ($H^{\pm}$) Higgs bosons.

According to the latest experimental results from both ATLAS and CMS, the presence of non-SM decay modes of the SM-like Higgs boson is not completely ruled out. Both experiments have set upper limits on the branching ratio (BR) of such non-SM decays which are 12% for ATLAS [5] and 16% for CMS [6]. The LHC experiments are expected to soon constrain the BRs of such non-SM decays beyond the 5%–10% level using indirect measurements [7,8]. There exist several BSM models that possess such non-SM decays of the SM-like Higgs boson: non-minimal scenarios of Supersymmetry [9] such as the next-to-minimal supersymmetric Standard Model and new minimal supersymmetric Standard Model (NMSSM/mMSSM) [10–13], models for dark matter (DM) [14–17], scenarios with first order electroweak (EW) phase transitions [18,19] and an extended Higgs sector [20,21]. It is then crucial to use LHC Higgs measurements to test BSM models that predict such exotic SM-like Higgs decays (i.e., into non-SM particles).

Previous phenomenological studies explored the potential presence of a lighter Higgs boson [22–33] and provided prominent signatures to probe the extended Higgs sector at the LHC. Direct detection of a light scalar h might be possible in a variety of production mechanisms and decay channels. In the 2HDM, if the heavy CP-even H is the observed SM-like Higgs boson, then H can decay into a pair of light CP-even Higgs states, $H \to hh$, or CP-odd ones, $H \to AA$. The phenomenology of such decays of the observed SM-like Higgs boson is studied in Refs. [32–35] for the case of the 2HDM, with an emphasis on the so-called type-I (see below). In this analysis, we focus primarily on the indirect generation of a pair light Higgs through the decay $H \to hh$, where the main production mode of H is via gluon fusion (ggF). This decay channel falls within an interesting class of processes that were probed at the LHC to explore the light Higgs within the sub-62 GeV range.

Following the discovery of the SM-like Higgs boson by ATLAS and CMS at the LHC in 2012, there have been several experimental searches for exotic decays of the SM-like Higgs through four fermions final states: $pp \to H \to XX \to f_1 f_1 f_2 f_2$, where $f_{1,2}$ are 2 light fermions such as muons, taus, or bottom quarks. Such a search clearly benefits from the large cross section $\sigma(pp \to H)$ as well as from the large BR of the exotic SM-like Higgs decay $H \to hh$ that could reach up to 10% in some BSM scenarios. In that spirit, the ATLAS and CMS collaborations have performed several searches looking for $\tau\tau\tau\tau$ [36,37], $\tau\tau\mu\mu$ [36,38–40], $b\bar{b}\mu\mu$ [36,41,42], $b\bar{b}\tau\tau$ [43,44], $eeee$ [45], $ee\mu\mu$ [45], and $\mu\mu\mu\mu$ [45–49], which have enabled one to set an upper limit on the BR of the X decay into any given 2 light fermions.

Motivated by the recent search for $b\bar{b}\tau\tau$ final states conducted by the CMS experiment [43,44], herein, we would like to address the study of signal and background for such a final state within the so-called 2HDM type-I. We first demonstrate that, within this framework, the production rate of $b\bar{b}\tau\tau$ via the process $\sigma(pp \to H) \times \mathrm{BR}(H \to hh) \times \mathrm{BR}(h \to b\bar{b}) \times \mathrm{BR}(h \to \tau\tau)$ could be substantial and then perform a feasibility study based on a signal-versus-background analysis using standard Monte Carlo (MC) simulation tools. It is found that the interesting parameter space could be either confirmed or disproved by a large dataset (say 3000 fb^{-1}), which can be attained at the High Luminosity LHC (HL-LHC) [50], with possible hints of such a signal already at run 3 of the LHC (for 300 fb^{-1}).

The paper is organized as follows: in Sec. II we give a brief review of the 2HDM and describe the theoretical and experimental constraints that are used. In Sec. III, we present some general features of the SM-like Higgs boson decays into two light Higgs bosons and further into $b\bar{b}\tau\tau$ final states over the parameter space of the inverted mass hierarchy scenario of the 2HDM type-I. In Sec. IV, we perform a detailed MC study of the feasibility of the signal process $gg \to H \to hh \to b\bar{b}\tau\tau$ at the current run 3 of the LHC and future HL-LHC stages. In Sec. V, we end this work with some conclusions.

II. THEORETICAL AND EXPERIMENTAL CONSTRAINTS

The 2HDM is obtained by extending the Higgs sector of the SM with an additional Higgs doublet field. Assuming that Φ_i ($i = 1, 2$) are the two $SU(2)_L$ Higgs doublets and $v_{1,2}$ are their vacuum expectation values (VEVs), the most general renormalizable potential which is invariant under $SU(2)_L \times U(1)_Y$ with a softly broken Z_2 symmetry is given by [21]:

$$V_{\rm Higgs}(\Phi_1,\Phi_2) = \lambda_1(\Phi_1^\dagger\Phi_1)^2 + \lambda_2(\Phi_2^\dagger\Phi_2)^2 + \lambda_3(\Phi_1^\dagger\Phi_1)(\Phi_2^\dagger\Phi_2) + \lambda_4(\Phi_1^\dagger\Phi_2)(\Phi_2^\dagger\Phi_1) + \frac{1}{2}\left[\lambda_5(\Phi_1^\dagger\Phi_2)^2 + \text{H.c.}\right] + m_{11}^2\Phi_1^\dagger\Phi_1 + m_{22}^2\Phi_2^\dagger\Phi_2 + \left[m_{12}^2\Phi_1^\dagger\Phi_2 - \text{H.c.}\right]. \quad (1)$$

By hermiticity, $\lambda_{1,2,3,4}$ as well as m_{11}^2 and m_{22}^2 are all real-valued. The parameters λ_5 and m_{12}^2 can be complex and can generate CP violation in the Higgs sector. However, in what follows, we assume that there is no such phenomenon.

After EW symmetry breaking (EWSB) takes place, from the 8 degrees of freedom initially present in Φ_1 and Φ_2, 3 are taken up by the ensuing Goldstone bosons to give masses to the gauge bosons $W^\pm$ and Z, so we are eventually left with 5 physical Higgs states. A pair of charged Higgs $H^\pm$, a CP-odd A and two CP-even states H and h (with $m_h < m_H$), as mentioned. One of the neutral CP-even Higgs states has to be identified with the 125 GeV SM-like Higgs particle observed at the LHC. In the present study, as intimated, we will assume $m_H = 125$ GeV while $m_h < m_H/2$.

The whole Higgs sector of the 2HDM is then parametrized by 7 parameters: e.g.,

$$m_{H^\pm}, \quad m_A, \quad m_H, \quad m_h, \quad \alpha, \quad \beta \quad \text{and} \quad m_{12}^2, \quad (2)$$

where α is the mixing angle between the CP-even components of the neutral Higgs states of the doublet fields while β is the mixing between the CP-odd components and is given by $\tan\beta = v_2/v_1$. As we are considering the scenario where H state is the 125 GeV scalar, the SM (alignment) limit is recovered when $\cos(\beta-\alpha) \approx 1$.

From the above Higgs potential, one can derive, in particular, the triple Higgs coupling Hhh needed for our analysis, as follows [51,52]:

$$Hhh = -\frac{g c_{\beta-\alpha}}{2 m_W s_{2\beta}^2}\left[(2m_h^2 + m_H^2)s_{2\alpha}s_{2\beta} - 2(3s_{2\alpha} - s_{2\beta})m_{12}^2\right], \quad (3)$$

where s_x and c_x are shorthand notations for $\sin x$ and $\cos x$, respectively. The coupling Hhh is proportional to $\cos(\beta-\alpha)$ which is close to unity in our scenario with H being the observed SM-like Higgs boson, as explained.

In the Yukawa sector, if we proceed to EWSB like in the SM, we end up with flavor changing neutral currents (FCNCs) at tree level. Such dangerous FCNCs can, however, be avoided by imposing a discrete Z_2 symmetry [53] by coupling each fermion type to only one of the Higgs doublets. As a consequence, there are four types of 2HDM [21], of which, in this study, we are interested only in the so-called type-I, wherein only the doublet Φ_2 couples to all fermions exactly as in the SM [21].

The neutral Higgs couplings to fermions can be obtained from the Yukawa Lagrangian and are given by [21]:

$$-\mathcal{L}_{\rm Yukawa} = \sum_{f=u,d,l}\frac{m_f}{v}\left(\frac{\cos\alpha}{\sin\beta}\bar{f}fh + \frac{\sin\alpha}{\sin\beta}\bar{f}fH\right). \quad (4)$$

As one can read from the above Lagrangian term, the CP-even neutral Higgs couplings to quarks and leptons are similar in the 2HDM type-I, since both are proportional to $\frac{1}{\sin\beta} \propto \frac{1}{\tan\beta}$: in particular, the H couplings to all fermions are suppressed if $\tan\beta \gg 1$.

The parameter space of the 2HDM (whatever the type) is limited by both theoretical and experimental constraints. The theoretical ones that have been imposed on the Higgs potential are as follows.

(i) Perturbativity constraints imply that all quartic coefficients of the Higgs potential satisfy the condition $|\lambda_i| \leq 8\pi$ $(i = 1,\ldots 5)$ [21].
(ii) Perturbative unitarity constraints require that $2 \to 2$ scattering processes involving Higgs and gauge bosons remain unitary at high energy [54–56].
(iii) Vacuum stability conditions require the Higgs potential to be bounded from below when the Higgs fields become large in any direction of the field space [57].

We have used the public code 2HDMC-1.7.0 [58] to check the above theoretical constraints.

We also take into account experimental constraints from Higgs analyses at lepton and hadron colliders (LEP, Tevatron, and LHC) as well as EW precision observables (EWPOs). Limits from flavor physics observables are also considered. Specifically, we have proceeded as follows.

(1) Exclusion limits at 95% confidence level (CL) from Higgs analyses at the aforementioned colliders are implemented via HiggsBounds-5.9.0 [59] and HiggsSignals-2.6.0 [60].
(2) We impose compatibility with the EWPOs by requiring the computed S, T, and U values [61–63] be within 2σ of the SM fit of [64], taking into account the full correlations among the three parameters.
(3) Constraints from B-physics observables are taken into account by using the public code SuperIso v4.1 [65], in particular, we have used the following measurements:
   (a) $\text{BR}(\bar{B} \to X_s\gamma)|_{E_\gamma < 1.6\,\text{GeV}} = (3.49 \pm 0.19) \times 10^{-4}$ [66],
   (b) $\text{BR}(B_s \to \mu^+\mu^-)_{(\text{LHCb})} = (3.09^{+0.46}_{-0.43}) \times 10^{-9}$ [67,68],
   (c) $\text{BR}(B_s \to \mu^+\mu^-)_{(\text{CMS})} = (3.83^{+0.38}_{-0.36}) \times 10^{-9}$ [69],
   (d) $\text{BR}(B^0 \to \mu^+\mu^-)_{(\text{LHCb})} = (1.2^{+0.8}_{-0.7}) \times 10^{-10}$ [67,68], and

(e) $\mathrm{BR}(B^0 \to \mu^+\mu^-)_{(\mathrm{CMS})} = (0.37^{+0.75}_{-0.67}) \times 10^{-10}$ [69].

B-physics observables enforce indirect experimental constraints on both $\tan\beta$ and $m_{H^\pm}$. The recent improved calculation of $\mathrm{BR}(\bar{B} \to X_s\gamma)$ within the 2HDM (type-II) leads to a stronger lower bound on the charged Higgs mass ($m_{H^\pm} \geq 800$ GeV (95% CL) [70]. This constraint is, however, relaxed in the 2HDM type-I, enabling the possibility of a light charged Higgs boson in a low mass range 100–200 GeV and $\tan\beta > 2$ [71]. A previous analysis [72] showed that $B_d \to \mu^\pm\mu^\mp$ (resp Δm_s) requires $\tan\beta > 3$ (resp $\tan\beta > 2.5$) [72]. In this study, we only considered the most constraining decays on the parameter space of the 2HDM type-I, namely $B_{d,s} \to \mu^+\mu^-$ and $B \to X_s\gamma$.

Lastly, additional constraints on light charged Higgs boson (i.e., $m_{H^\pm} < 200$ GeV) have been taken into account. At the LHC, both ATLAS and CMS Collaborations have carried out a variety of searches for light charged Higgs bosons ($m_{H^\pm} < m_{\mathrm{top}}$) in top quark decay, in different final states, i.e., $H^\pm \to \tau\nu$ [73–79], cs [80–82], cb [83], $W^\pm A(\to \mu^+\mu^-)$[84]. These experiments have set upper limits on charged Higgs production and decay rates. Lately, the ATLAS group carried out a search for $H^+ \to cb$ in $t\bar{t}$ events, with 139 fb^{-1} of data at $\sqrt{s} = 13$ TeV [85]; limits on $\mathrm{Br}(t \to H^+b) \times \mathrm{Br}(H^\pm \to cb)$ in the range 0.15% to 0.42% were obtained.

III. NUMERICAL RESULTS

As mentioned repeatedly, in this study, we focus on the inverted mass hierarchy scenario, where the heaviest Higgs is identified as the observed 125 GeV at the LHC. We then scan randomly the 2HDM parameters over the ranges of Table I.

The important theoretical constraints on the 2HDM arise from tree-level perturbartive unitarity and electroweak vacuum stability. The parameter space allowed by these two constraints can be enlarged, if we allow for a mass term breaking the imposed Z_2 symmetry softly, thus choosing a nonzero m_{12}^2 [86]. The choice of $m_{12}^2 = m_h^2 c_\beta s_\beta$ is motivated to ensure a compliance with the theoretical and experimental constraints. On the other hand, after conducting a general scan over $\sin(\beta-\alpha) \in [-0.25, 0.25]$, and varying the remaining parameters in the ranges given in Table 1, we found that the positive values of $\sin(\beta-\alpha)$ are ruled out after applying HiggsSignal, which enforces constraints derived from Higgs signal strength measurements (depicted by red points in Fig. 1). We therefore restrict ourselves to negative values

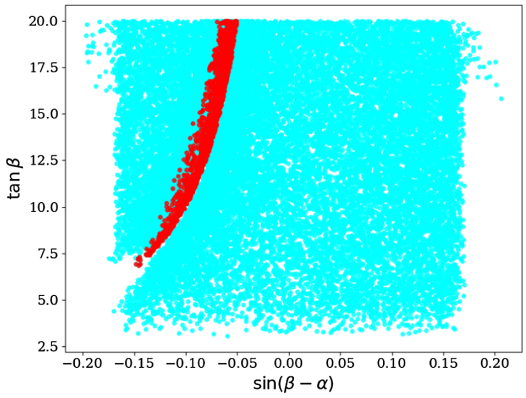

FIG. 1. The parameter space of the 2HDM type-I over the $(\sin(\beta-\alpha), \tan\beta)$ plane. Cyan points satisfy all theoretical constraints and pass HiggsBounds test. Red points are allowed by all theoretical requirements and experimental constraints imposed by HiggsBounds and HiggsSignal.

of $\sin(\beta-\alpha)$ and narrowed down our scan to the following range: $\sin(\beta-\alpha) \in [-0.25, -0.05]$.

Upon meeting the theoretical requirements and the constraints derived from past and ongoing experimental studies, described in Sec. II, we illustrate in Figs. 2 and 3 the BRs for different decay modes of the light Higgs: $h \to \gamma\gamma, b\bar{b}$, and $\tau\tau$. Away from the fermiophobic limit, where the light Higgs couplings to fermions (κ_f^h) are very suppressed ($c_\alpha/s_\beta \to 0$) and the diphoton decay of the light Higgs state can become significant, the total width of the h state is clearly dominated by $h \to b\bar{b}$, over the entire 2HDM type-I parameter space, with a BR of 85%, followed by the decay into $\tau\tau$ with BR of order ∼8%. The decay rate of $h \to b\bar{b}$ drops to 45% when κ_f^h approaches very small values ($\lesssim 0.001$) and m_h is around 15 GeV. Furthermore, the partial width $\Gamma(h \to b\bar{b})$ exhibits a suppression near the $2m_b$ threshold and, therefore, $h \to \gamma\gamma$ can closely compete with $h \to b\bar{b}$ there. Within the same parameter space, the decay width of the charged Higgs ($\Gamma_{H^\pm}$) is dominated by the bosonic decay channel $H^\pm \to W^\pm h$ (see Fig. 4), which is kinematically open in the mass range $m_h \in [10, 62]$ GeV, whereas the fermionic decays are suppressed. The branching ratio $\mathrm{BR}(H^\pm \to W^\pm h)$ enjoys an enhancement of the coupling $H^\mp W^\pm h$ which is proportional to $\cos(\beta-\alpha) \approx 1$. Previous phenomenological studies in the framework of 2HDM type-I motivated the charged Higgs bosonic decays [87–89] to search for light charged Higgs, we therefore will not be exploring the charged Higgs scenario any further in this analysis.

TABLE I. The input parameters of the 2HDM are tabulated and their scan ranges given. (Note that we have fixed $m_H = 125$ GeV).

Parameter	m_h (GeV)	m_A (GeV)	$m_{H^\pm}$ (GeV)	$\sin(\beta-\alpha)$	$\tan\beta$	m_{12}^2 (GeV^2)
Range	[10, 62]	[62, 100]	[96, 200]	$[-0.25, -0.05]$	[2, 25]	$m_h^2 \cos\beta \sin\beta$

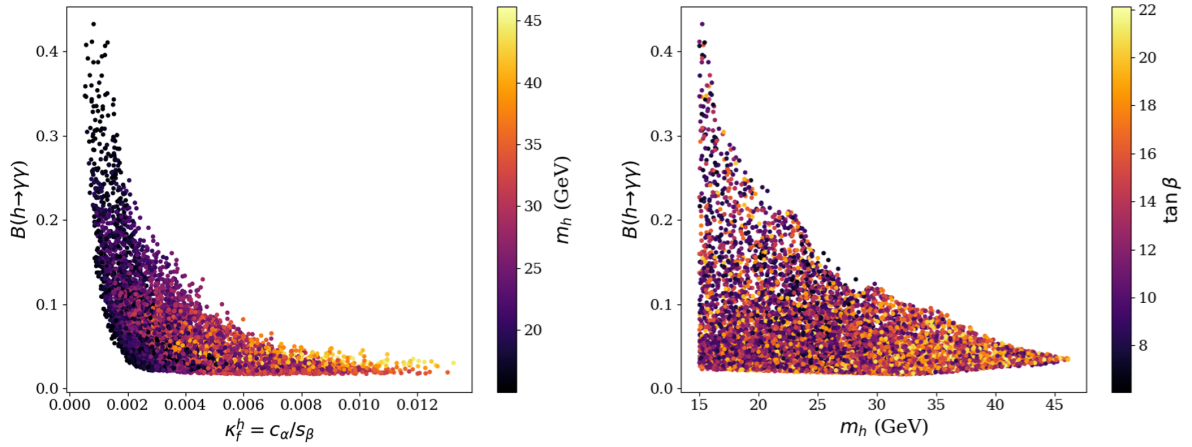

FIG. 2. $\mathrm{BR}(h \to \gamma\gamma)$ as a function of κ_f^h vs. m_h (left panel) and as a function of m_h vs $\tan\beta$ (right panel) vs m_h.

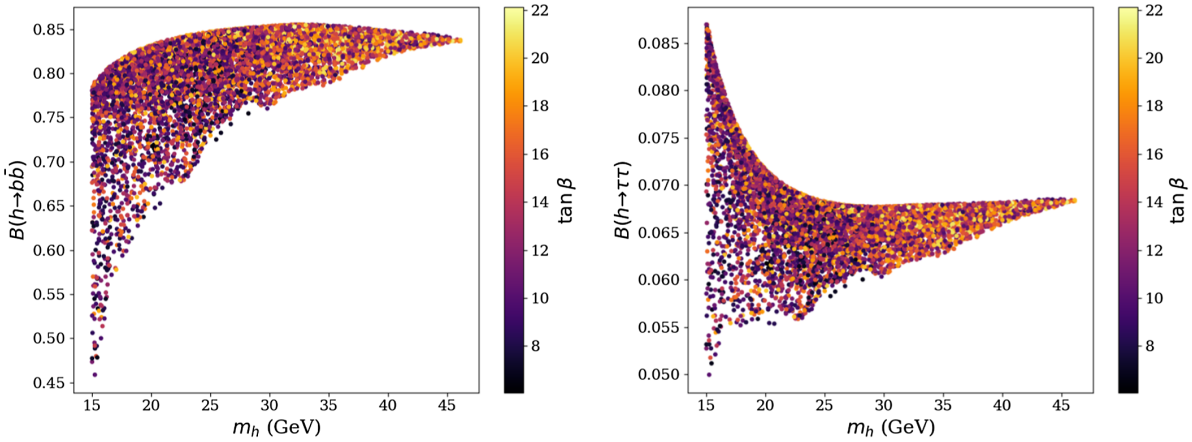

FIG. 3. $\mathrm{BR}(h \to b\bar{b})$ (left panel) and $\mathrm{BR}(h \to \tau\tau)$ (right panel) vs m_h and $\tan\beta$.

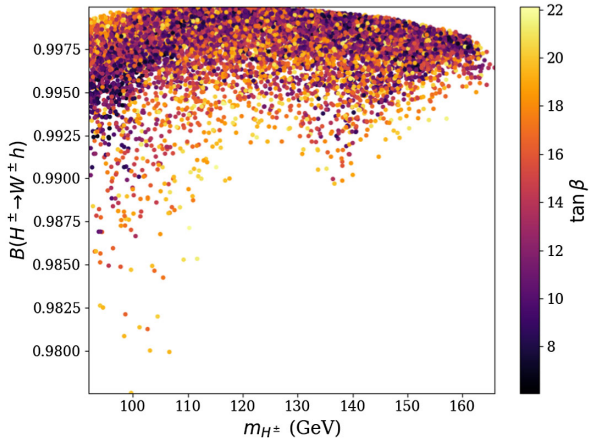

FIG. 4. $\mathrm{BR}(H^\pm \to W^\pm h)$ vs $m_{H^\pm}$ and $\tan\beta$ in the 2HDM type-I.

Figure 5 shows the overall cross section of the process $pp \to H \to hh \to b\bar{b}\tau\tau$, wherein the main channel for producing the SM-like Higgs boson H is the gluon-gluon fusion mechanism. Here, $\mathrm{BR}(h \to b\bar{b}), \mathrm{BR}(h \to \tau\tau)$ and $\mathrm{BR}(H \to hh)$ are also displayed. Since the decay width of the SM-like Higgs (Γ_H) is of the order of a few MeV ($\Gamma_H^{\mathrm{ATLAS}} = 4.6^{+2.6}_{-2.5}$ MeV [90] and $\Gamma_H^{\mathrm{CMS}} = 3.2^{+2.4}_{-1.7}$ MeV [91]), one can assume the narrow width approximation (NWA)[1] and then write the complete production times decay cross section as follows:

$$\sigma_{b\bar{b}\tau\tau} = \sigma(gg \to H) \times \mathrm{BR}(H \to hh) \times \mathrm{BR}(h \to b\bar{b}) \times \mathrm{BR}(h \to \tau\tau), \tag{5}$$

[1]The same applies to the h state, which would be even narrower.

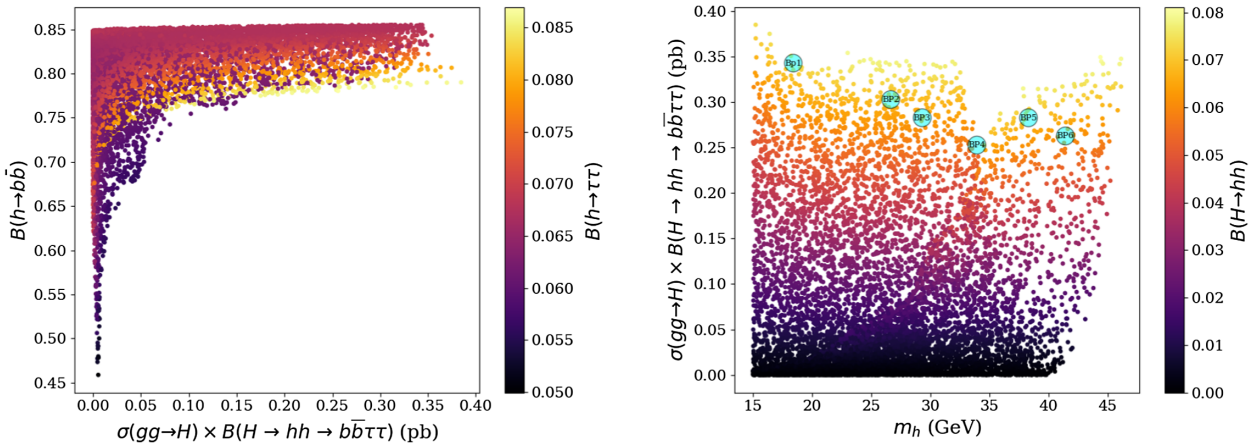

FIG. 5. BR($h \to b\bar{b}$) as a function of $\sigma(gg \to H \to hh \to b\bar{b}\tau\tau)$ vs. BR($h \to \tau\tau$) (left panel) and $\sigma(gg \to H \to hh \to b\bar{b}\tau\tau)$ as a function of m_h vs. BR($H \to hh$) (right panel).

where $\sigma(gg \to H)$ is the H production rate computed (here) at leading order (LO) using SusHi 1.7.0 [92–94] at the center-of-mass energy of 13 TeV. (The N^{3}LO QCD corrections will be considered through a K-factor [95,96], see below.) As shown previously in Eq. (3), the trilinear Higgs coupling Hhh is proportional to $\cos(\beta - \alpha)$. In the inverse mass hierarchy configuration of the 2HDM type-I, current data drive $\cos(\beta - \alpha)$ to closely approach 1 and thus BR($H \to hh$) is not suppressed. However, it is observed that the BR of the SM-like Higgs boson (H) decaying into a pair of light Higgs bosons (hh) remains below 10% when the decay channel becomes kinematically accessible. This limitation arises from the precise measurements of the Higgs boson couplings, which impose stringent constraints on exotic decays of the Higgs boson, i.e., into BSM particles and/or undetected final states. As mentioned previously, the ATLAS and CMS collaborations have set, respectively, an upper limit of 12% [5] and 16% [6] on BR($H \to$ BSM) at 95% CL, using LHC run 2 data.[2] Further searches for light pseudoscalars, where m_a ranged between 15 and 62 GeV, imposed upper limits on light Higgs decay rates, i.e., $H \to aa(hh)$. Recently, the CMS group reported a search for $H \to aa \to 4\gamma$ with 132 fb^{-1} of data [99]; upper limits on B($H \to aa \to 4\gamma$) ranging between 0.80 fb for $m_a = 15$ GeV to 0.26 fb for $m_a =$ 62 GeV were obtained. The ATLAS collaboration searched for $H \to aa$ in $b\bar{b}\mu\mu$ final state with 139 fb^{-1} of data at $\sqrt{s} = 13$ GeV; upper limits in the range $(0.2\text{–}4.0) \times 10^{-4}$ were placed on $B(H \to aa \to b\bar{b}\mu\mu)$ [100]. As stated above, a recent search for exotic Higgs decay in $b\bar{b}\tau\tau$ and $b\bar{b}\mu\mu$ final states has been performed by the CMS group with 138 fb^{-1} of data [42]. Upper limits on BR($H \to aa \to \mu\mu b\bar{b}$) and BR($H \to aa \to b\bar{b}\tau\tau$) are in the range $(0.17\text{–}3.3) \times 10^{-4}$ and $(1.7\text{–}7.6) \times 10^{-2}$, respectively. Our surviving points were checked against the upper limits on BR($H \to hh \to 4\gamma$ [99], $b\bar{b}\tau\tau$ [42], $\mu\mu b\bar{b}$ [42], $\mu\mu\tau\tau$) [40].[3] Compatibly with these constraints, we find that the cross section for the process $gg \to H \to hh \to b\bar{b}\tau\tau$ reaches its maximum value of 0.4 pb when BR($h \to b\bar{b}$), BR($h \to \tau\tau$) and BR($H \to hh$) are at their maximum values. Over the parameter region allowing for this, we have marked several Benchmark Points (BPs) amenable to MC simulation, which are listed in Table II. As stated above, both ATLAS and CMS searched for $H \to aa$ in different final states, i.e., $b\bar{b}\tau\tau$ final state. Such decay topology is well motivated in many BSM such as next-to-minimal 2HDM. In the 2HDM-I, the decay channel $H \to aa \to b\bar{b}\tau\tau$ is kinematically open when $m_a \in [10, 62]$ GeV, and the branching ratios of $H \to aa$, $a \to b\bar{b}$ and $a \to \tau\tau$ could respectively reach 10%, 85% and 7% as shown in Fig. 6, leading to $\sigma_{H\to aa\to b\bar{b}\tau\tau} \approx \sigma_{H\to hh\to b\bar{b}\tau\tau}$. However, one cannot explore low mass range where m_a is below 40 GeV [101,103] given that such a region is already excluded by LEP search for $h \to aa$ [104] and Z width (Γ_Z) measurements [105,106].

An additional scan is performed to further explore the 2HDM type-I parameter space, and to test the sensitivity of $\tan\beta$ and m_h to the current experimental searches. After performing a general scan, we have selected a point with

[2]Recently, the ATLAS collaboration also performed a combination of run 1 and 2 direct searches for invisible Higgs decays, where several production modes of the SM-like Higgs boson are considered [97]. An upper bound of 10.7% (7.7%) on BR($H \to$ invisible) at the 95% CL has been observed (expected). The CMS collaboration has also lately presented the combination of a search for $H \to$ invisible with the SM-like Higgs state produced in association with a top-antitop pair (i.e., $pp \to t\bar{t}H$) or a vector boson (i.e., $pp \to VH$) using 138 fb^{-1} of data from both run 1 and 2: the combined upper limit on BR($H \to$ invisible) is 15% at 95 C.L. [98].

[3]A similar work has been carried out in a previous study [101], where we used EasyNData [102] to digitise the upper bounds from published papers in order to check our parameter space against the aforementioned exclusions.

TABLE II. The cross sections $\sigma_{b\bar{b}\tau\tau} \equiv \sigma(gg \to H) \times \mathrm{BR}(H \to hh) \times \mathrm{BR}(h \to b\bar{b}) \times \mathrm{BR}(h \to \tau\tau)$ for our BPs are given for the collision energy $\sqrt{s} = 13$ TeV alongside the BRs for the decay channels $H \to hh$, $h \to b\bar{b}$ and $\tau\tau$. The unit of all masses is GeV. Here, $m_H = 125$ GeV, and in the values of cross section $\sigma_{b\bar{b}\tau\tau}$ the K-factor has been taken into consideration.

BP	m_h (GeV)	m_a (GeV)	$m_H^{\pm}$ (GeV)	$\sin(\beta-\alpha)$	$\tan\beta$	$\sigma_{b\bar{b}\tau\tau}$ (pb)	$\mathrm{BR}(H \to hh)$	$\mathrm{BR}(h \to b\bar{b})$	$\mathrm{BR}(h \to \tau\tau)$
BP1	17.67	73.70	184.51	−0.053	19.68	0.34	0.07	0.81	0.076
BP2	25.9	80.61	171.88	−0.064	16.71	0.3	0.068	0.84	0.068
BP3	28.56	94.46	155.45	−0.11	9.09	0.28	0.065	0.85	0.067
BP4	33.20	88.29	99.75	−0.076	14.42	0.25	0.058	0.85	0.067
BP5	37.56	88.88	188.64	−0.064	16.45	0.28	0.072	0.8	0.064
BP6	40.68	88.37	144.39	−0.054	19.37	0.26	0.063	0.82	0.066
BP7	47.27	98.91	165.58	−0.10	11.34	0.38	0.074	0.85	0.074
BP8	54.03	98.91	165.58	−0.10	11.28	0.40	0.083	0.84	0.07
BP9	43.44	98.91	165.58	−0.10	10.43	0.34	0.077	0.80	0.065
BP10	49.39	98.91	165.58	−0.10	10.41	0.21	0.056	0.78	0.065

high m_a ($H \to aa$ is not open kinematically) and large $B(H \to hh \to b\bar{b}\tau\tau)$ from the surviving parameter space (marked with green color in Fig. 7). We then used the values of its parameters (i.e., $m_{H^{\pm}} = 165.58$ GeV, $m_A = 98.9$ GeV, $\sin(\beta-\alpha) = -0.10$, and $m_{12}^2 = 154$ GeV^2) to run another scan while m_h and $\tan\beta$ are varied randomly as shown in Table I.

We show in the left panel of Fig. 8 the allowed region resulting from passing the theoretical constraints, indicated by blue color. The points that meet the theoretical requirements and also align with experimental data are highlighted in red color. To gain a better understanding of this restricted parameter space, which is limited to a narrow range of values of $\tan\beta$, we highlight, in the right panel of Fig. 8, the excluded $\tan\beta$ region and the corresponding searches. For values of $\tan\beta$ below 9, the CMS search for exotic decays in the $b\bar{b}\tau\tau$ [44] final state has excluded the mass range where $m_h < 50$ GeV whereas the region where $m_h > 50$ GeV is excluded by the LEP search for $e^+e^- \to hA \to b\bar{b}b\bar{b}$ [104]. The ATLAS search for events with at least three photons (i.e., 3γ) targeting the process $pp \to H \to hh \to 4\gamma$ [107] has excluded the region with $8.6 \leq \tan\beta < 10.3$ when m_h ranged between $40 \leq m_h \leq 61.7$ GeV. The large $\tan\beta$ region is excluded by both HiggsSignal (HS) (brown areas) and by the following experimental searches: $e^+e^- \to ha \to b\bar{b}b\bar{b}$ [104], $pp \to hh \to b\bar{b}\tau\tau$ [44] and $pp \to H \to hh \to b\bar{b}\mu\mu$ [108]. The allowed parameter space in the mass range [40, 54.8] GeV corresponds to $\tan\beta \in [10.3-11.4]$. There are few allowed points around $m_h \approx 62$ when $\tan\beta \approx$ 9.8–10.1. This can be seen clearly in Figs. 9 and 10 (indicated by yellow points).

We show in Fig. 9 the different BRs within the described parameter space. Similarly to Fig. 2, the dominant channel within the parameter space where $m_h < 60$ GeV is $h \to b\bar{b}$, with a BR that can reach up to 85%. The second prominent channel is $h \to \tau\tau$ with a BR that goes up to 8%. Another interesting observation is that the fermionic decay rates of $h \to b\bar{b}$ and $\tau\tau$ remain relatively unaffected by $\tan\beta$ variations. For large $\tan\beta$,

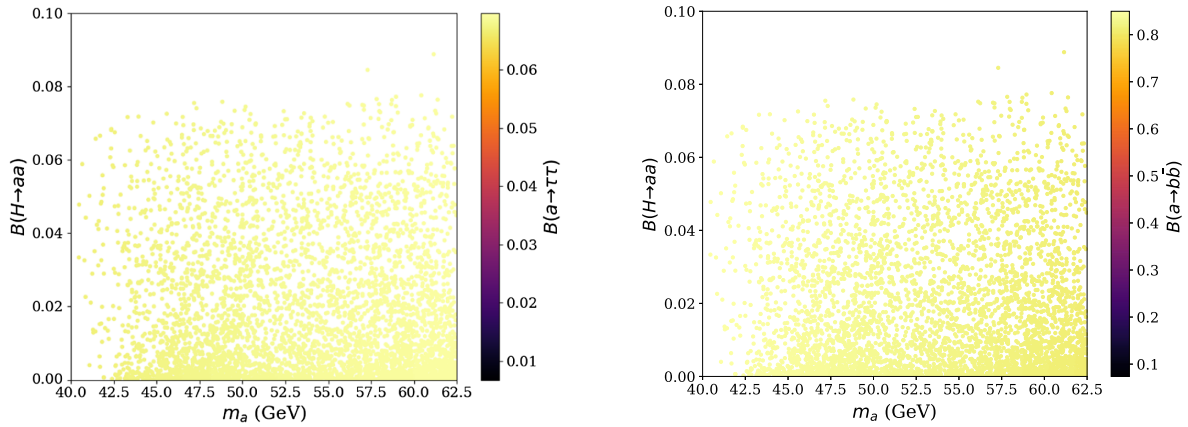

FIG. 6. $\mathrm{BR}(H \to aa)$ as a function of m_a vs. $\mathrm{BR}(a \to \tau\tau)$ (left panel) and $\mathrm{BR}(a \to b\bar{b})$ (right panel) in the 2HDM type-I.

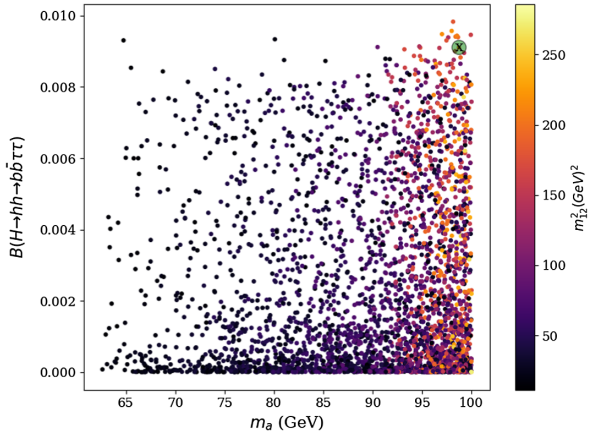

FIG. 7. $\mathrm{BR}(H \to hh \to b\bar{b}\tau\tau)$ as a function of m_a vs m_{12}^2 within the allowed parameter space of the 2HDM type-I.

the Yukawa couplings[4] become suppressed, leading the BRs of the light Higgs state decaying into fermions to become fairly independent on the values of $\tan\beta$ within the considered parameter space.

In Fig. 10, we present the production cross section of the SM-like Higgs state H times its decay BR into $b\bar{b}\tau\tau$ via hh, i.e., $\sigma(gg \to H) \times \mathrm{BR}(H \to hh \to b\bar{b}\tau\tau)$, within the specified parameter space. The maximum value of this product is observed to be 0.4 pb, which occurs, again, when $\mathrm{BR}(H \to hh)$, $\mathrm{BR}(h \to \tau\tau)$ and $\mathrm{BR}(h \to b\bar{b})$ all reach their maximum values within the considered parameter space. Similarly to the previous scenario, we have selected a few BPs to perform a MC simulation. These BPs are carefully chosen to cover a range of interesting scenarios and to explore various aspects of the model, see Table II.

IV. FEASIBILITY STUDY AT THE LHC RUN 3

In our MC analysis, we focus on the $b\bar{b}\tau\tau$ final state, where both τ leptons decay into either an electron or a muon, along with their respective neutrinos. To distinguish between the decays of the τ particles, we use the short-hand notations τ_e and τ_μ to represent the channels $\tau \to e\bar{\nu}_e\nu_\tau$ and $\tau \to \mu\bar{\nu}_\mu\nu_\tau$, respectively. The final states $\tau_e\tau_e$ and $\tau_\mu\tau_\mu$ are neglected in order to suppress the significant contamination from Drell-Yan (DY) background events. In Fig. 11, we present the Feynman diagram of the signal process, where effective vertices are considered for the gluon-gluon-Higgs coupling and for leptonic tau decay [109].

We use MadGraph-v.3.4.2 [110] to generate parton-level events of both signal and background processes. To account for the τ decays, we use the TauDecay library [109].[5] The QCD corrections are taken into account by using K-factors for (what we will prove to be) the two main background processes $Z(\to \tau_e\tau_\mu)b\bar{b}$ [111] and $t\bar{t}$ [112]: specifically, $K = 1.4$ for both $b\bar{b}Z$ and $t\bar{t}$. The K-factor for the signal production process $gg \to H$ is taken as $K = 2.5$, which includes the N^{3}LO QCD corrections of Refs. [95,96]. We then pass the events to PYTHIA8 [113] for parton showering, fragmentation/hadronization and heavy flavor decays. Then, we use DELPHES-3.5.0 [114] with a standard CMS card to simulate the detector response. Finally, we employ MadAnalysis 5 [115] to apply cuts and to conduct the kinematic analysis. As mentioned already, the BPs and the corresponding parameter values used to generate MC samples of events for the signal process are given in Table II, where, as usual, the collision energy at the proton-proton level is assumed to be 13 TeV.

In order to generate signal and background events efficiently, we apply the following kinematic cuts at parton level:

$$p_T(b) > 10\,\mathrm{GeV}, \quad p_T(l) > 5\,\mathrm{GeV}, \quad E_T^{\mathrm{miss}} > 5\,\mathrm{GeV},$$
$$|\eta(b,l)| < 2.5, \Delta R(ll,bl,bb) > 0.3, \quad H_T < 70\,\mathrm{GeV}.$$

Where H_T is computed over all partons.

The LO cross sections of all background processes considered in our initial MC analysis are given in Table III. As intimated, it is found that the dominant background processes arise from top pair production ($t\bar{t}$) and $Z(\to \tau_e\tau_\mu)b\bar{b}$, so that we will simulate only these two processes in our final (detector level) analysis.

A. Parton level analysis

In Fig. 12, the p_T distributions of the leading and subleading leptons as well as of the b-(anti)quarks for the signal are displayed. These spectra provide insights into the transverse momentum of final-state particles involved in the signal process, in order to guide our final analysis at detector level.

On the one hand, it is observed that the leading and subleading leptons originating from the light Higgs decay (recall that $m_h < 62.5$ GeV) tend to have lower transverse momentum, indicating that they are relatively softer when compared with the leading (subleading) b-(anti)quarks from the same light Higgs state (owing to neutrinos carrying away energy). In particular, the peak value of p_T of the subleading lepton is less than 10 GeV, which means a stiff (detector level) cut on $p_T(l)$ may lead to a severe loss of signal events. On the other hand, since the b-tagging efficiency decreases with p_T, then one should expect that a stiff (detector level) cut on, especially, the subleading b-jet can also lead to a severe loss of signal events. In short, these factors call for a dedicated trigger choice, that we will illustrate below.

In Fig. 13, we show the leading (subleading) lepton and b-(anti)quark of different background processes at parton level. It is observed that the subleading lepton from

[4]Notice that $\kappa_h^f = \sin(\beta-\alpha) + \cot\beta\cos(\beta-\alpha) \approx \sin(\beta-\alpha)$ for large $\tan\beta$, with $\sin(\beta-\alpha) = -0.10$.

[5]The TauDecay package has been added to the UFO file of the 2HDM type-I.

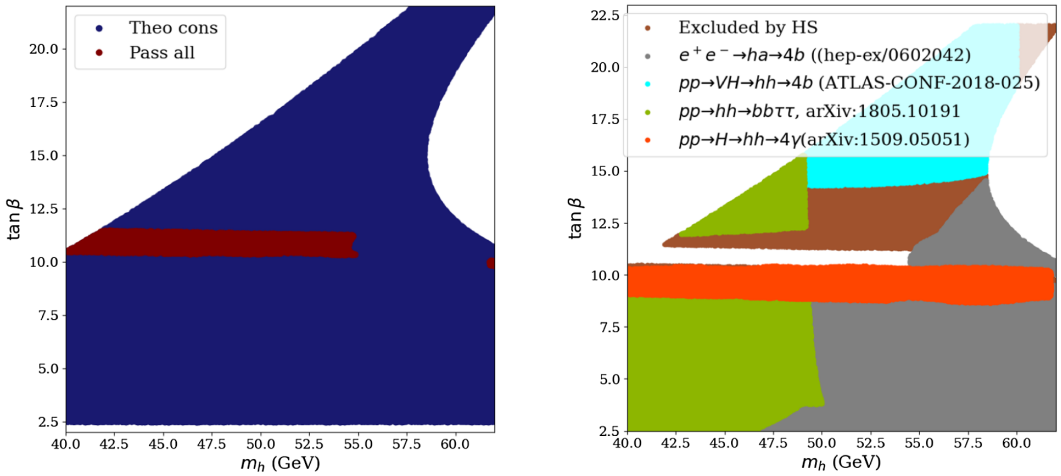

FIG. 8. Allowed (left panel) and excluded (right panel) parameter space over the $(m_h, \tan\beta)$ plane. Here, $m_{H^\pm} = 165.58$ GeV, $m_A = 98.9$ GeV, $\sin(\beta - \alpha) = -0.10$, $m_{12}^2 = 154$ GeV^2.

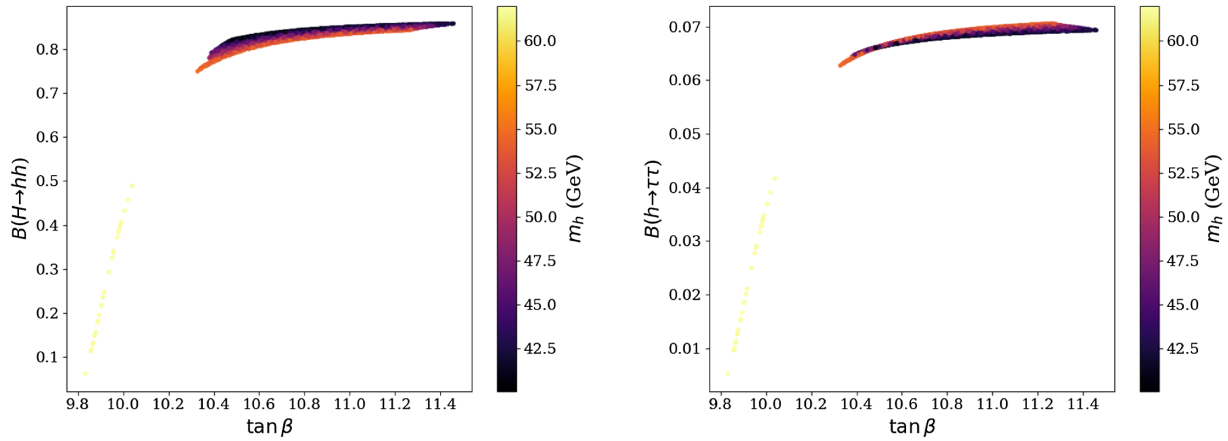

FIG. 9. $\mathrm{BR}(h \to b\bar{b})$ (left panel) and $\mathrm{BR}(h \to \tau\tau)$ (right panel) as a function of $\tan\beta$ vs m_h. Here, $m_{H^\pm} = 165.58$ GeV, $m_A = 98.9$ GeV, $\sin(\beta - \alpha) = -0.10$, $m_{12}^2 = 154$ GeV^2.

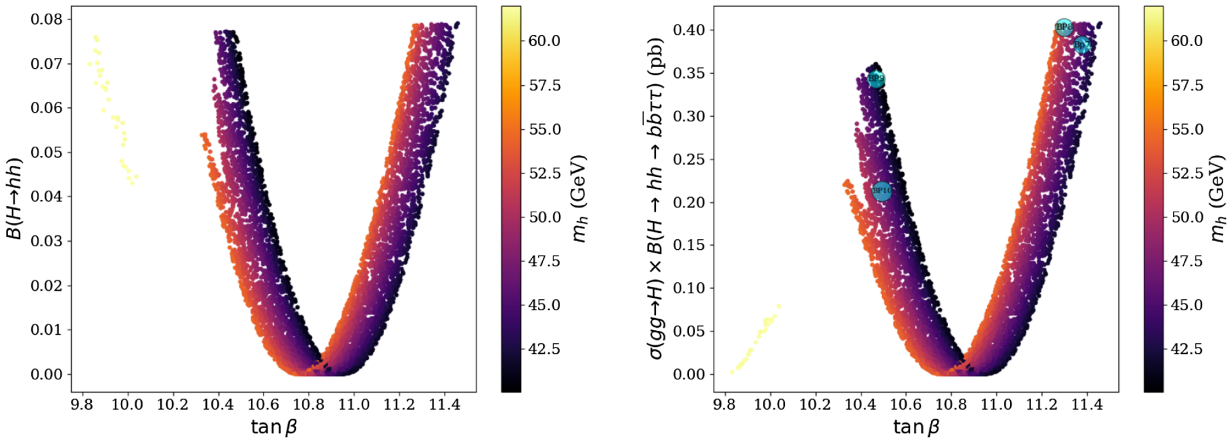

FIG. 10. $\mathrm{BR}(h \to hh)$ (left panel) and $\sigma(gg \to H) \times \mathrm{BR}(H \to hh \to b\bar{b}\tau\tau)$ (right panel) as a function of $\tan\beta$ vs m_h.

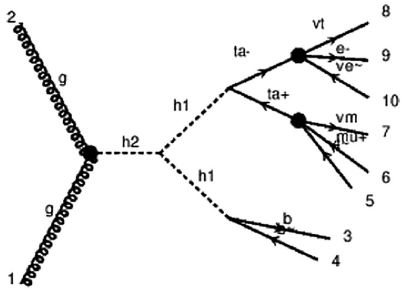

FIG. 11. Feynman diagram for the process $gg \to H \to hh \to b\bar{b}\tau_e\tau_\mu$. Here, $h_2 \equiv H$ and $h_1 \equiv h$.

$Z(\to b\bar{b})\tau_e\tau_\mu$ can be very soft, just like the subleading lepton from the signal events. Similarly, the subleading b-(anti)quark from $Z(\to \tau_e\tau_\mu)b\bar{b}$ can be very soft, which can then mimic the subleading b-(anti)quark of the signal events. Thus, this renders even more important the accurate choice of a dedicated trigger for this analysis. However, as intimated, from Table III, it is clear that the dominant background processes are $pp \to Z(\to \tau_e\tau_\mu)b\bar{b}$ and $pp \to t\bar{t}$. Therefore, in order to discover the signal process, the key task is to ultimately suppress these two backgrounds. Armed with the knowledge acquired at the parton level, we will investigate below how to suppress these two types of noise most effectively at the detector level.

B. Detector level analysis

We only consider events with two b-jets and two leptons of different flavor with opposite charges (i.e., $e^{\mp}\mu^{\pm}$) in the final state. Given that both (leading and subleading) leptons in the signal events are soft, as illustrated in Fig. 14, it will be necessary to suitably adjust the transverse momentum (p_T) thresholds of the leading electron (e) and subleading muon (μ). By reducing these p_T thresholds, one can include more signal events and then increase the acceptance so to mitigate the potential significant loss of signal events due to the softness of the leptons, especially the subleading one. Consequently, the trigger choice could lead to a more comprehensive view of the final state and potentially improve the overall sensitivity of the analysis.

TABLE III. The LO background cross sections are given for the collision $\sqrt{s} = 13$ TeV. The K-factors mentioned in the text has not been included here but will be used to compute the final significances, albeit limitedly to the second and last processes (i.e., the two dominant noises).

Background process	σ (pb)
$pp \to Z(\to b\bar{b})Z(\to ll)$, $l = (e, \mu, \tau_{e,\mu})$	0.009
$pp \to Z(\to ll)b\bar{b}$, $l = (e, \mu, \tau_{e,\mu})$	6.1
$pp \to Z(\to b\bar{b})ll$, $l = (e, \mu, \tau_{e,\mu})$	0.015
$pp \to ZW^{\pm}j, W^{\pm} \to l\nu_l (l = e, \mu, \tau_{e,\mu})$	0.0051
$pp \to t\bar{t} \to e^{\pm}\mu^{\mp}b\bar{b} + E_T^{\text{miss}}$	0.28

Events featuring tau decays into leptons ($\tau_e\tau_\mu$) are collected by electron and muon triggers. The CMS cross trigger [116,117] relies on the presence of both an electron (e) and a muon (μ), where the leading lepton has a p_T threshold of 23 GeV and the subleading one has a $p_T >$ 12 GeV for an electron or 8 GeV for a muon [42,44]. This trigger is limited by p_T thresholds in the level-1 (L1) trigger selection due to the limited L1 bandwidth available. The double electron trigger is similarly limited. Recently, in run 3, CMS has overcome this limitation for electron pairs that are close together, for example from B meson decays, by placing tighter topological selection on the two electrons L1 objects. This borrows from established approaches already used in double muon triggers searching for low p_T muons from B meson decays. By applying similar topological approaches to an electron muon trigger, it would seem possible to develop a reasonably efficient L1 selection targeting 10 GeV close by electron muon pairs with a rate in the ∼2–5 kHz range at nominal run 3 luminosities. A L1 selection with such a bandwidth is feasible to be deployed in run 3 if there is sufficient will on the experiment's side to do so and would be easily achievable at the HL-LHC. At the high level trigger (HLT) selection stage, the rate should be manageable and if not, scouting and parking techniques [118,119] can be used if the rate of the selection is too much to be included in the standard physics stream. Electrons and muons from τ decays are then selected after satisfying the following requirements:

$$p_T^e > 10\,\text{GeV}, \quad p_T^\mu > 8\,\text{GeV}, \quad |\eta^e| < 2.4, \quad |\eta^\mu| < 2.4.$$

Lepton candidates must also satisfy isolation criteria, which ensure that the amount of activity in a cone of radius $R = 0.4$ centered on the muon (electron) direction is smaller than 20% (15%) of $p_T^\mu(p_T^e)$. For the jets candidates, we employ the anti-k_T algorithm [120] to cluster detector-level objects with a jet radius parameter $\Delta R = 0.4$ and $p_{T,j}^{\min} = 10$ GeV (for both light- and b-jets).[6] All events are required to have two b-tagged jets with $p_T(b_1/b_2) >$ 10 GeV (where $p_T(b_{1(2)})$ represents the b-jet with highest (lowest) p_T) and $|\eta^b| < 2.4$.[7] The reconstruction of b-jet with jets of $p_T < 20$ GeV might be very challenging due to the degradation in b-tagging efficiency over lower transverse momentum ranges, however, it is still worthwhile to investigate how the b-tagging efficiency changes in

[6]Note that our results are rather stable against a different choice of jet clustering algorithm, like the Cambridge-Aachen one [121,122].

[7]Jets are b-tagged with an average efficiency ($\varepsilon_{b/b}$) of ∼60% (i.e., $\varepsilon_{b/b} = 0.85 \times \tanh(0.0025 \times p_T) \times (25.0/(1 + 0.063 \times p_T))$ [123], with p_T is the transverse momentum of the jet.)

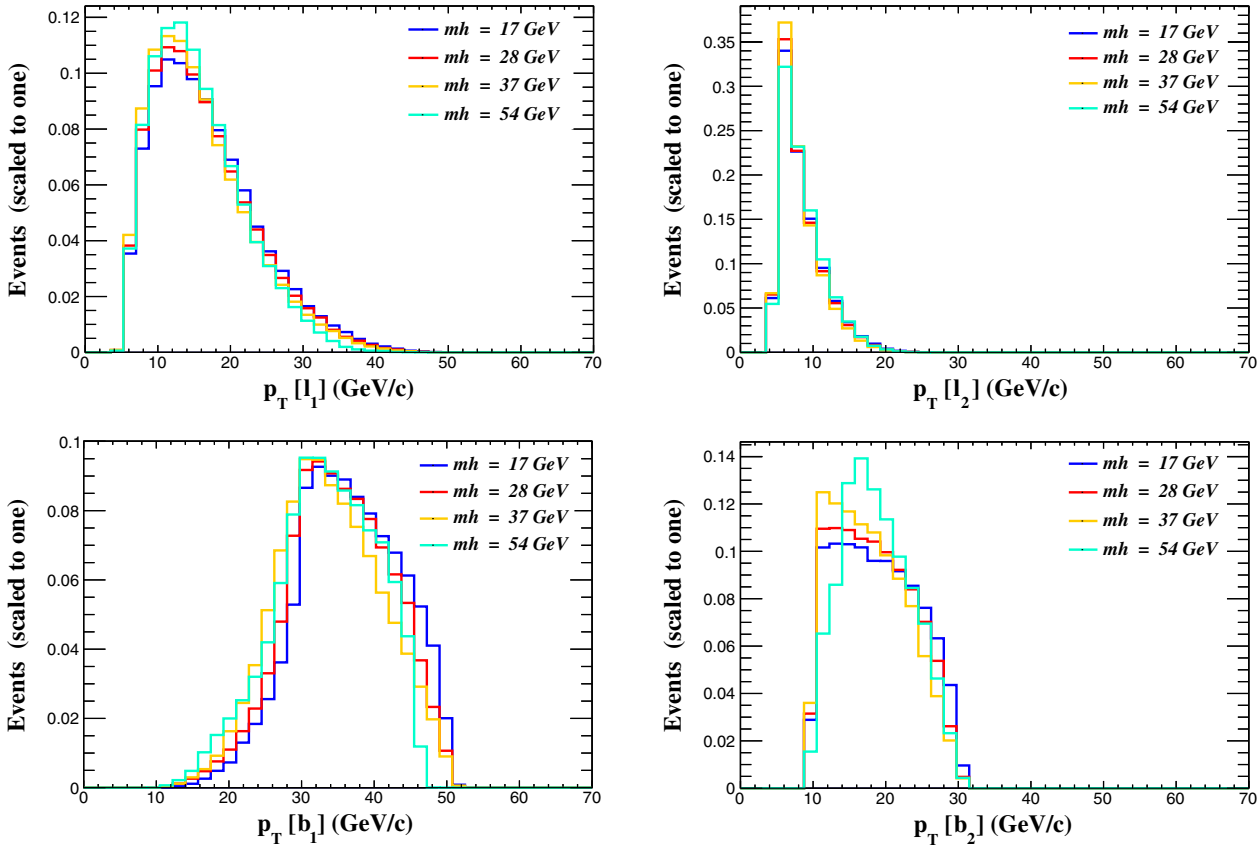

FIG. 12. The p_T distributions of the leading (subleading) lepton (top panel) and leading (subleading) b-(anti)quark (bottom panel) for different signal BPs at are shown at parton level, see Table III.

response to different p_T thresholds, so that we will do so below.

To increase the sensitivity of our analysis, we will explore various kinematic distributions which include the invariant mass of the b-jets ($m_{b\bar{b}}$) as well as the constructed mass from the τ leptons decay products and the b-jets (m_T^H). These variables are typically low for signal events because the objects originate from a 125 GeV Higgs state. Conversely, they generally have higher values for background events, where the objects do not arise from a decay of a (rather light) resonance. Such kinematic features can serve to efficiently discern between signal and background events in our analysis.

Figure 15 displays the invariant mass distribution of the b-jets for different BPs. Notably, $m_{b\bar{b}}$ aligns closely to the light Higgs mass (m_h) for each BP. We present in Fig. 16 the transverse mass distributions constructed from the two charged leptons and E_T^{miss}. As anticipated, the peak structure in these distributions is shifted from the expected light Higgs mass for the selected BPs ($m_T^{ll} \lesssim m_h$) due to the missing contribution of the neutrinos. The m_T^{ll} variable is defined from p_{ll} (the total four-momentum of the leptons) and E_T^{miss} as

$$m_T^{ll} = \sqrt{p_{ll}^0 E^0 - |p_{ll}^T||E^T|\cos(\phi_{ll,E_T^{\text{miss}}})}. \tag{6}$$

For the sake of convenience, we denote E_T^{miss} as (E^0, E^T, p_z), where p_z is the unknown z-component of the missing momentum and E^T is a 2D vector defined in the (x, y) plane perpendicular to the beam direction. Here, $\phi_{ll,E_T^{\text{miss}}}$ denotes the perpendicular angle between the dilepton system and E_T^{miss}.

In Fig. 17, we show the transverse mass constructed from the two b-jets, the two leptons and E_T^{miss}. The variable m_T^H is defined from the two b-jet four-momenta $p_{b\bar{b}} = p(b) + p(\bar{b})$, p_{ll} and E_T^{miss}. To define m_T^H, we first express the visible momentum, which equals $p_{\text{vis}} = p_{b\bar{b}} + p_{ll}$, so that we have

$$m_T^H = \sqrt{p_{\text{vis}}^0 E^0 - |p_{\text{vis}}^T||E^T|\cos(\phi_{\text{vis},E_T^{\text{miss}}})}, \tag{7}$$

where $\phi_{\text{vis},E_T^{\text{miss}}}$ denotes the perpendicular angle between visible momentum and E_T^{miss}. Clearly, fully reconstructing the signal can yield a significant improvement in the signal-to-background ratio. Selecting events with low m_T^H will efficiently mitigate the background contamination arising from the $t\bar{t}$ process, which is characterized by a large missing transverse momentum.

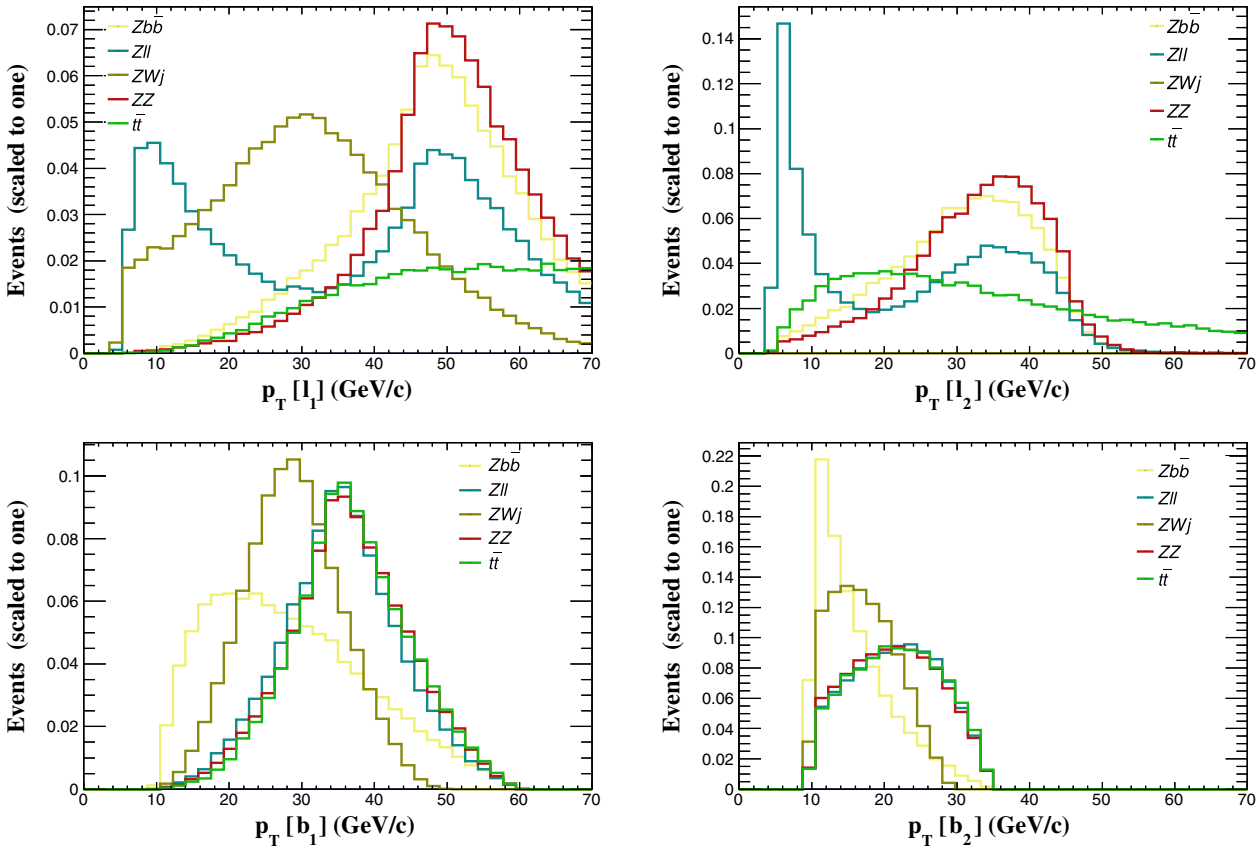

FIG. 13. The p_T distributions of the leading (subleading) lepton and b-(anti)quark of different background processes are shown at parton level, see Table III.

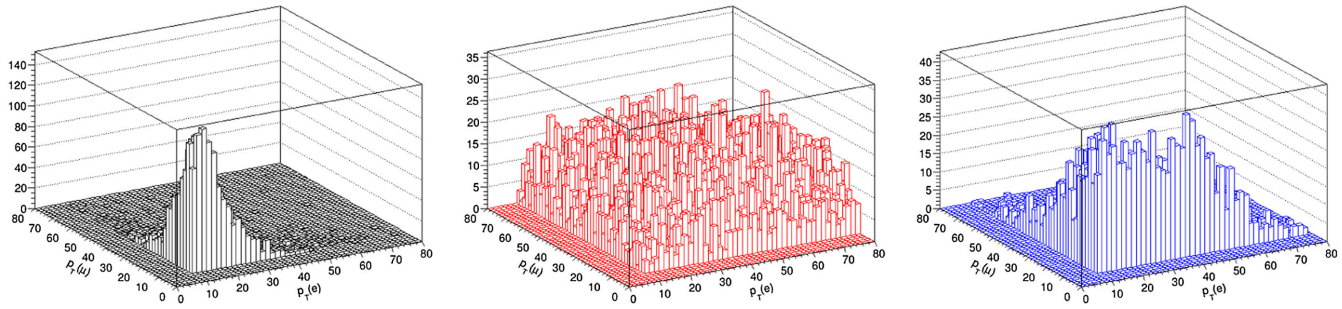

FIG. 14. Correlations between the p_T of the leading and subleading leptons for signal (black), $t\bar{t}$ (red) and $b\bar{b}Z(\to \tau_e\tau_\mu)$ (blue) are shown at detector level.

The requirement for precisely two b-tagged jets in each event is notably a tight condition due to the soft transverse momentum (p_T) spectrum of b-jets and the limited efficiency of the b-tagging algorithm. These b-tagging techniques [124,125] operate at peak efficiency when b-jets possess a large transverse momentum of at least 20 GeV. However, at this threshold, a significant loss of the signal would occur particularly in scenarios involving low Higgs masses below 60 GeV as a result of the kinematics. Therefore, to examine how the efficiencies can change, especially the b-tagging one, we will compare the impact of the following three cuts, which we regard as preselection rules:

$$p_T(b_1/b_2) > 15/10 \text{ GeV}, \qquad p_T(b_1/b_2) > 20/15 \text{ GeV}, \qquad p_T(b_1/b_2) > 20/20 \text{ GeV}. \tag{8}$$

The results are provided in Tables IV–VI, respectively. (In these tables, to estimate the number of events, we assume that the LHC collision energy at proton-proton level is $\sqrt{s} = 13$ TeV and the integrated luminosity is that of run 3,

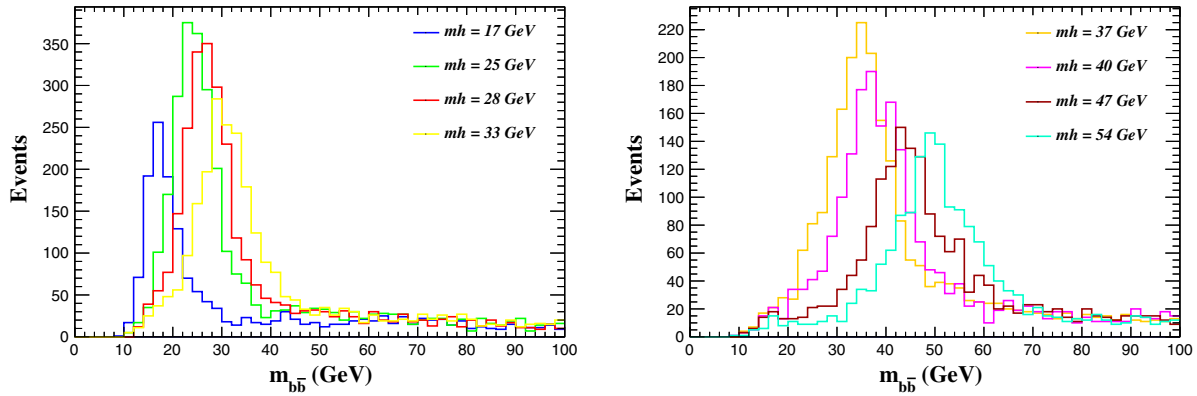

FIG. 15. The distributions of $m_{b\bar{b}}$ for different BPs are shown at detector level.

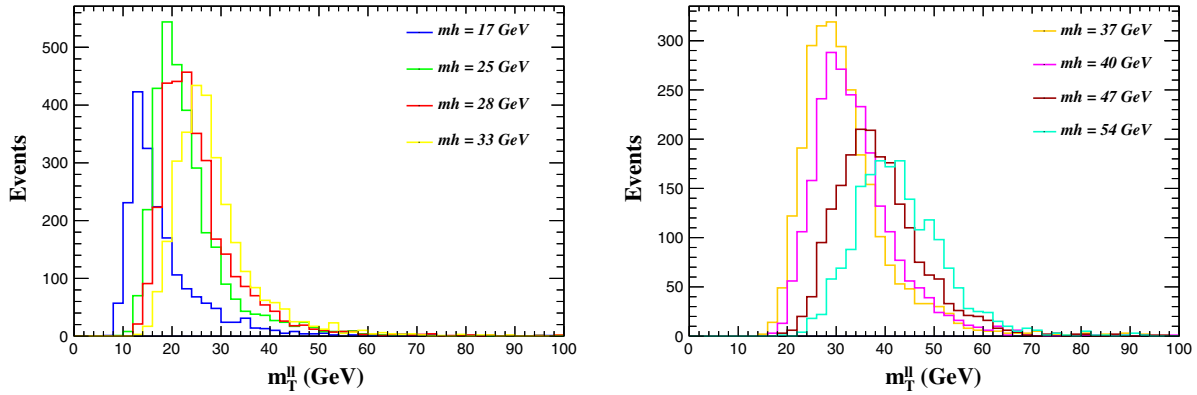

FIG. 16. The distributions of m_T^{ll} for different BPs are shown at detector level.

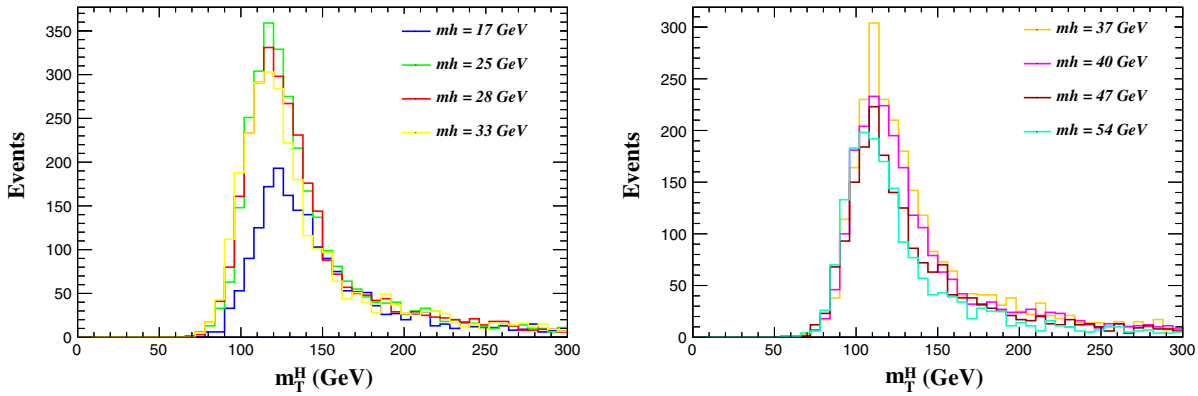

FIG. 17. The distributions of m_T^H for different BPs are shown at detector level.

i.e., 300 fb^{-1}.) Meanwhile, the leptons from τ decays are collected with thresholds at $p_T(e/\mu) = 10/8$ GeV, which can guarantee a sufficiently large fraction of signal events to be retained. We now discuss the effect of three preselections introduced in Eq. (8) in turn, each of which is supplemented by the same cutflow, which has been devised following the kinematic analysis performed at detector level.

In Table IV, we adopt the following preselection cuts:

$$p_T(b_1) > 15 \text{ GeV}, \qquad p_T(b_2) > 10 \text{ GeV}, \qquad p_T(e/\mu) = 10/8 \text{ GeV}. \tag{9}$$

As stated above, several requirements on events are enforced. The first one is that each event contains exactly

TABLE IV. Event rates of the signal with $\sqrt{s} = 13$ TeV and integrated luminosity 300 fb^{-1} for different BPs are shown as a function of our cutflow. The preselection cuts are as given in Eq. (9).

BP	BP1	BP2	BP3	BP4	BP5	BP6	BP7	BP8	BP9	BP10
m_h (GeV)	17.67	25.9	28.56	33.20	37.56	40.68	47.27	54.03	43.44	49.39
NoE ($\mathcal{L}$, σ)	912.86	727.65	687.432	573.3	771.74	769.18	1086.62	1528.8	900.000	771.750
$e^{\pm}\mu^{\mp}$	156.934	151.874	141.094	114.84	146.44	136.2	160.54	204.94	151.226	111.163
m_Z-veto	156.934	151.874	141.094	114.84	146.44	136.2	160.54	204.94	151.226	111.163
$2b$-jets	33.0	42.88	39.98	32.32	38.84	34.94	40.9	53.2	38.09	26.28
65 GeV $< m_T^H <$ 125 GeV	11.78	20.56	19.1	16.42	20.4	18.78	23.02	33.92	20.95	15.15
$\Delta m_h < 0.5$	8.1	15.88	15.16	12.96	16.24	14.84	18.18	27.34	16.95	12.015
$m_T^{ll} <$ 62.5 GeV	8.1	15.86	15.14	12.94	16.24	14.84	18.18	27.18	16.63	11.98
$m_{bb} <$ 62.5 GeV	8.1	15.86	15.12	12.94	16.24	14.76	18.18	27.04	16.60	11.97

TABLE V. Event rates of the signal with $\sqrt{s} = 13$ TeV and integrated luminosity 300 fb^{-1} for different BPs are shown as a function of our cutflow. The preselection cuts are as given in Eq. (10).

BP	BP1	BP2	BP3	BP4	BP5	BP6	BP7	BP8	BP9	BP10
m_h (GeV)	17.67	25.9	28.56	33.20	37.56	40.68	47.27	54.03	43.44	49.39
NoE ($\mathcal{L}$, σ)	912.86	727.65	687.432	573.3	771.74	769.18	1086.62	1528.8	900.000	771.750
$e^{\pm}\mu^{\mp}$	156.934	151.874	141.094	114.84	146.44	136.2	160.54	204.94	151.226	111.163
m_Z-veto	156.934	151.874	141.094	114.84	146.44	136.2	160.54	204.94	151.226	111.163
$2b$-jets	23.9	32.38	30.8	23.24	29.36	25.76	28.56	40.036	28.125	18.714
65 GeV $< m_T^H <$ 125 GeV	7.76	13.72	13.372	11.32	13.82	12.38	14.58	22.56	13.890	9.470
$\Delta m_h < 0.5$	5.232	11.36	10.77	8.94	10.76	9.84	11.92	17.56	10.973	7.373
$m_T^{ll} <$ 62.5 GeV	5.232	11.36	10.76	8.92	10.76	9.82	11.9	17.5	10.961	7.363
$m_{bb} <$ 62.5 GeV	5.232	11.34	10.75	8.92	10.76	9.78	11.9	17.38	10.948	7.363

TABLE VI. Event rates of the signal with $\sqrt{s} = 13$ TeV and integrated luminosity 300 fb^{-1} for different BPs are shown as a function of our cutflow. The preselection cuts are as given in Eq. (11).

BP	BP1	BP2	BP3	BP4	BP5	BP6	BP7	BP8	BP9	BP10
m_h (GeV)	17.67	25.9	28.56	33.20	37.56	40.68	47.27	54.03	43.44	49.39
NoE ($\mathcal{L}$, σ)	912.86	727.65	687.432	573.3	771.74	769.18	1086.62	1528.8	900.000	771.750
$e^{\pm}\mu^{\mp}$	156.934	151.874	141.094	114.84	146.44	136.2	160.54	204.94	151.226	111.163
m_Z-veto	156.934	151.874	141.094	114.84	146.44	136.2	160.54	204.94	151.226	111.163
$2b$-jets	13.6	20.38	19.02	15.3	17.86	16.02	18.34	23.7	17.39	11.06
65 GeV $< m_T^H <$ 125 GeV	2.68	7.16	6.84	5.72	6.84	6.16	6.14	11.38	6.80	4.19
$\Delta m_h < 0.5$	1.86	5.5	5.56	4.5	5.32	4.8	5.54	8.2	5.25	3.13
$m_T^{ll} <$ 62.5 GeV	1.86	5.5	5.56	4.48	5.32	4.8	5.52	8.2	5.25	3.13
$m_{bb} <$ 62.5 GeV	1.86	5.5	5.56	4.48	5.32	4.78	5.52	8.12	5.23	3.13

two leptons ($\ell^{\pm}\ell^{\mp} = e^{\pm}\mu^{\mp}$). Events with lepton-pair invariant mass with 10 GeV of the Z-boson mass are rejected ("m_Z−veto"). This cut will not affect the signal but can act on background events. Following the selection of 2 tagged b-jets, we apply an additional selection criterion on the transverse mass (m_T^H) requiring that 65 GeV $< m_T^H <$ 125 GeV. This is reasonable as the Jacobian peak of the transverse mass of the SM-like Higgs boson is bound to be smaller than SM-like Higgs boson mass itself, $m_H = 125$ GeV. For the signal events, where both $b\bar{b}$ and $\tau\tau$ originate from the decay of the light Higgs, h, in principle, we expect the reconstructed masses $m_{b\bar{b}}$ and m_{ll}^T to be closely correlated. In reality, a major difference between the two reconstructed masses, as shown in Figs. 15 and 16, arises due to the z-component of the missing energy which is absent in m_{ll}^T, which prevents us from finding the precise invariant mass of the light Higgs boson decaying into $\tau\tau$. In order to quantify the difference between $m_{b\bar{b}}$ and m_{ll}^T, we have then introduced a new variable (Δm_h), i.e., $\Delta m_h \equiv (m_{b\bar{b}} - m_{ll}^T)/m_{ll}^T$. A cut on $\Delta m_h < 0.5$ would help removing background events since in the latter there is no correlation between $m_{b\bar{b}}$ and $m_{\tau\tau}$. Lastly, we set cuts on m_T^{ll}

TABLE VII. Event rates of the two dominant background processes with $\sqrt{s} = 13$ TeV and integrated luminosity 300 fb^{-1} as a function of our cutflow. The preselection cuts are as given in Eqs. (9)–(11).

Process		$Zb\bar{b}$			$t\bar{t}$	
NoE($\mathcal{L}$, σ)		2562000			117600	
$p_T(b_1/b_2)$ (GeV)	15/10	20/15	20/20	15/10	20/15	20/20
$e^{\pm}\mu^{\mp}$	15836.8	15836.8	15836.8	61413.5	61413.5	61413.5
m_Z-veto	15801.4	15801.4	15801.4	54511.6	54511.6	54511.6
$2b$-jets	1512.57	1059.63	503.558	16871.4	13778.6	8843.26
65 GeV $< m_T^H <$ 125 GeV	272.439	154.314	33.2724	35.2954	18.8916	3.087
$\Delta m_h < 0.5$ GeV	117.072	30.0678	⋯	17.5266	7.6678	⋯
$m_T^{ll} < 62.5$ GeV	117.072	30.0678	⋯	14.2366	6.125	⋯
$m_{bb} < 62.5$ GeV	117.072	30.0678	⋯	14.2366	6.125	⋯

TABLE VIII. Significances for our signal against the two dominant backgrounds with $\sqrt{s} = 13$ TeV and integrated luminosity 300 fb^{-1} (left) as well as 3000 fb^{-1} (right). The preselection cuts are as given in Eqs. (9)–(11).

	Significance (Σ), $\mathcal{L} = 300$ fb^{-1}			Significance (Σ), $\mathcal{L} = 3000$ fb^{-1}		
BP	15/10 (GeV)	20/15 (GeV)	20/20 (GeV)	15/10 (GeV)	20/15 (GeV)	20/20 (GeV)
BP1	0.68	0.81	1.36	2.15	2.56	4.30
BP2	1.30	1.64	2.34	4.11	5.18	7.39
BP3	1.24	1.57	2.35	3.92	4.96	7.43
BP4	1.07	1.32	2.11	3.38	4.17	6.67
BP5	1.33	1.57	2.3	4.20	4.96	7.27
BP6	1.22	1.44	2.18	3.85	4.55	6.89
BP7	1.48	1.71	2.34	4.68	5.40	7.39
BP8	2.14	2.37	2.84	6.76	7.49	8.9
BP9	1.36	1.59	2.28	4.3	5.02	7.2
BP10	1.0	1.11	1.76	3.16	3.51	5.56

and m_{bb} to be half of m_H in order to capture the SM-like Higgs boson decaying into two light Higgs bosons, $H \to hh$, in the signal events. Combining all kinematic information so far, we summarize in Table IV the event rates after meeting the event selection requirements.

Table V presents the results based on the following preselection cuts, while considering the same kinematic cuts as in Table IV:

$$p_T(b_1) > 20 \text{ GeV}, \qquad p_T(b_2) > 15 \text{ GeV}, \qquad p_T(e/\mu) = 10/8 \text{ GeV}. \tag{10}$$

Here, the same comments on the event kinematics of the signal apply as for the previous table.

In Table VI, we show the cutflow results by adopting the preselection cuts:

$$p_T(b_1) > 20 \text{ GeV}, \qquad p_T(b_2) > 20 \text{ GeV}, \qquad p_T(e/\mu) = 10/8 \text{ GeV}. \tag{11}$$

(Again, the same comments on the event kinematics of the signal apply as for the previous table.)

When comparing the results given in Tables IV–VI, particularly the number of events after requiring two tagged b-jets, it is found that the larger the p_T thresholds of the b-jets, the smaller the number of signal events which can pass the preselection cuts. This loss is an expected outcome for a light Higgs within the sub-50 GeV range, and it aligns with our expectations. However, it is too early to conclude that with loose cuts one can maximise the sensitivity since the effects of background have to be taken into account, which is what we are going to do next.

In Table VII we show the cutflow results for the two major background processes. Here, it is noted that two mass observables, i.e., m_T^H and Δm_h, can greatly suppress background events. Another interesting observation is that, although the number of signal events is comparatively smaller with the preselection cut 20/20 GeV on the two tagged b-jets, the background events can be almost completely removed in this case, which eventually leads to a better sensitivity to our signal process.

This is explicitly shown in Table VIII, where the significances $\Sigma = \frac{\mathcal{N}_S}{\sqrt{\mathcal{N}_S + \mathcal{N}_B}}$[8] for 300 fb^{-1} and 3000 fb^{-1} of each BP are shown. As mentioned above, the

[8] $\mathcal{N}_S$ and $\mathcal{N}_B$ are, respectively, the number of the signal and background events after applying the kinematic cuts discussed in the text.

preselection cut 20/20 GeV can yield a better significance, so it is the one we would recommend for the actual analysis. Altogether, although it is not feasible to discover or rule out all these BPs at run 3 of the LHC, they are all within full reach of the HL-LHC.

V. CONCLUSIONS

The type-I is an intriguing realization of the 2HDM as it allows for the so-called inverted mass hierarchy scenario, wherein the Higgs boson discovered at the LHC on 4 July 2012 can be identified as the heaviest *CP*-even Higgs state of this construct, H, with a mass of 125 GeV or so and couplings to fermions and gauge bosons similar to those predicted in the SM. Such a configuration specifically implies that there is then a lighter *CP*-even Higgs state, h, into pairs of which the heavy one can decay: i.e., via $H \to hh$. Needless to say, this can be realized without contradicting any of the theoretical requirements of self-consistency of the 2HDM or current experimental results, whether coming for measurements of the discovered Higgs boson or null searches for companions to it. In fact, the latter have primarily been concentrating on other realizations of the 2HDM, where only the standard mass hierarchy is actually possible (i.e., $m_h \approx 125$ GeV $< m_H$), thereby altogether missing out on the possibility of optimizing searches for very light neutral Higgs states in general. Specifically, here, by looking for $H \to hh$ signals in the 2HDM type-I, we have concentrated on the following mass range: 15 GeV $< m_h < m_H/2$.

The production of the heavy *CP*-even Higgs state (the SM-like Higgs boson) at the LHC was pursued via gluon-gluon fusion, $gg \to H$, indeed, the dominant channel, while we have focused on the $hh \to b\bar{b}\tau\tau$ decay pattern, where the two heavy leptons where tagged through their (different flavor) electron and muon decays. By performing a sophisticated MC analysis of signal versus background, we have shown that both run 3 of the CERN machine and its HL-LHC phase can offer sensitivity to this 2HDM type-I signal, in the presence of very low mass trigger thresholds (on the electrons and muons) already implemented for run 3 and also possible at the HL-LHC. We have done so by adopting several BPs capturing representative m_h values over the aforementioned interval after a fine scanning of the whole 2HDM type-I parameter space, of which they are therefore representative examples amenable to further scrutiny by the LHC collaborations. Finally notice that, if the collision energy of the LHC increases from 13 TeV to 14 TeV, the production rate of the signal process $gg \to H$ can increase by 10%, as shown in [95] (with the dominant backgrounds, $t\bar{t}$ and $Zb\bar{b}$, scaling similarly or less), lending further scope to our analysis in the near future.

ACKNOWLEDGMENTS

We would like to thank Sam Harper for his invaluable input and discussions around the trigger analysis. S. M. is supported in part through the NExT Institute and the STFC Consolidated Grant No. ST/L000296/1. C. H. S-T.(S. S.) is supported in part(full) through the NExT Institute. S. S. acknowledges the use of the IRIDIS High Performance Computing Facility, and associated support services at the University of Southampton, in the completion of this work. Y. W.'s work is supported by the Natural Science Foundation of China Grant No. 12275143, the Inner Mongolia Science Foundation Grant No. 2020BS01013 and the Fundamental Research Funds for the Inner Mongolia Normal University Grant No. 2022JBQN080. Q. S. Y. is supported by the Natural Science Foundation of China under the Grants No. 11875260 and No. 12275143.

APPENDIX

Additional kinematic variables can serve to further discriminate the Higgs signal from background events in the low mass range. Leptons arising from light Higgs decays demonstrate small opening angles, whereas those from $t\bar{t}$ (large missing transverse momentum) and $Z(\to \tau\tau)b\bar{b}$ (emitted back-to-back) would be large. Therefore, requiring a small opening angle between the two leptons, along with a small angle between the missing transverse momentum and the leptons would reduce the background processes. This is exemplified in Fig. 18. However, we did not pursue this here.

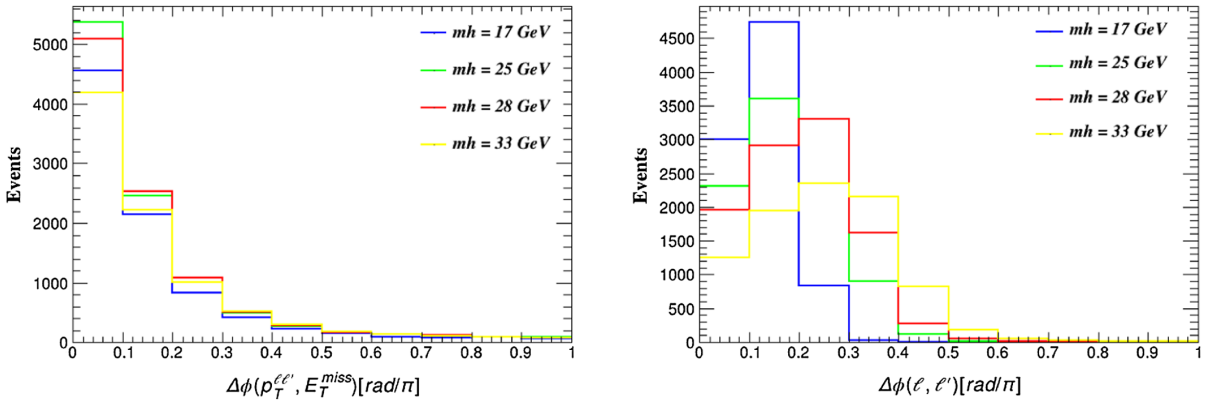

FIG. 18. Opening angles distributions between the two leptons $\Delta\phi(l, l')$ (left panel) and between the missing transverse momentum and the leptons $\Delta\phi(p_T^{ll'}, E_T^{\text{miss}})$ (right panel) for the signal, with $(ll' = e^{\pm}\mu^{\mp})$.

[1] Georges Aad *et al.*, Observation of a new particle in the search for the Standard Model Higgs boson with the ATLAS detector at the LHC, Phys. Lett. B **716**, 1 (2012).

[2] Serguei Chatrchyan *et al.*, Observation of a new boson at a mass of 125 GeV with the CMS experiment at the LHC, Phys. Lett. B **716**, 30 (2012).

[3] F. Englert and R. Brout, Broken symmetry and the mass of gauge vector mesons, Phys. Rev. Lett. **13**, 321 (1964).

[4] Peter W. Higgs, Broken symmetries and the masses of gauge bosons, Phys. Rev. Lett. **13**, 508 (1964).

[5] G. Aad *et al.* (ATLAS Collaboration), A detailed map of Higgs boson interactions by the ATLAS experiment ten years after the discovery, Nature (London) **607**, 52 (2022); **612**, E24 (2022).

[6] Armen Tumasyan *et al.*, A portrait of the Higgs boson by the CMS experiment ten years after the discovery, Nature (London) **607**, 60 (2022).

[7] A. Liss and J. Nielsen, Physics at a High-Luminosity LHC with ATLAS (2013).

[8] Projected performance of an upgraded CMS detector at the LHC and HL-LHC: Contribution to the Snowmass process, in Snowmass 2013: Snowmass on the Mississippi (2013).

[9] Stefano Moretti and Shaaban Khalil, *Supersymmetry Beyond Minimality: From Theory to Experiment* (CRC Press, 2019).

[10] A. Dedes, C. Hugonie, S. Moretti, and K. Tamvakis, Phenomenology of a new minimal supersymmetric extension of the Standard Model, Phys. Rev. D **63**, 055009 (2001).

[11] Bogdan A. Dobrescu and Konstantin T. Matchev, Light axion within the next-to-minimal supersymmetric standard model, J. High Energy Phys. 09 (2000) 031.

[12] Ulrich Ellwanger, John F. Gunion, Cyril Hugonie, and Stefano Moretti, Towards a no lose theorem for NMSSM Higgs discovery at the LHC (2003).

[13] Radovan Dermisek and John F. Gunion, Escaping the large fine tuning and little hierarchy problems in the next to minimal supersymmetric model and $h \to aa$ decays, Phys. Rev. Lett. **95**, 041801 (2005).

[14] Maxim Pospelov, Adam Ritz, and Mikhail B. Voloshin, Secluded WIMP dark matter, Phys. Lett. B **662**, 53 (2008).

[15] Patrick Draper, Tao Liu, Carlos E. M. Wagner, Lian-Tao Wang, and Hao Zhang, Dark light Higgs, Phys. Rev. Lett. **106**, 121805 (2011).

[16] Seyda Ipek, David McKeen, and Ann E. Nelson, A renormalizable model for the Galactic center gamma ray excess from dark matter annihilation, Phys. Rev. D **90**, 055021 (2014).

[17] Abdesslam Arhrib, Yue-Lin Sming Tsai, Qiang Yuan, and Tzu-Chiang Yuan, An updated analysis of inert Higgs doublet model in light of the recent results from LUX, PLANCK, AMS-02 and LHC, J. Cosmol. Astropart. Phys. 06 (2014) 030.

[18] Stefano Profumo, Michael J. Ramsey-Musolf, and Gabe Shaughnessy, Singlet Higgs phenomenology and the electroweak phase transition, J. High Energy Phys. 08 (2007) 010.

[19] Nikita Blinov, Jonathan Kozaczuk, David E. Morrissey, and Carlos Tamarit, Electroweak baryogenesis from exotic electroweak symmetry breaking, Phys. Rev. D **92**, 035012 (2015).

[20] T. D. Lee, A theory of spontaneous T violation, Phys. Rev. D **8**, 1226 (1973).

[21] G. C. Branco, P. M. Ferreira, L. Lavoura, M. N. Rebelo, Marc Sher, and Joao P. Silva, Theory and phenomenology of two-Higgs-doublet models, Phys. Rep. **516**, 1 (2012).

[22] P. M. Ferreira, Rui Santos, Marc Sher, and Joao P. Silva, Could the LHC two-photon signal correspond to the heavier scalar in two-Higgs-doublet models?, Phys. Rev. D **85**, 035020 (2012).

[23] Sanghyeon Chang, Sin Kyu Kang, Jong-Phil Lee, Kang Young Lee, Seong Chan Park, and Jeonghyeon Song, Comprehensive study of two Higgs doublet model in light of the new boson with mass around 125 GeV, J. High Energy Phys. 05 (2013) 075.

[24] Sanghyeon Chang, Sin Kyu Kang, Jong-Phil Lee, Kang Young Lee, Seong Chan Park, and Jeonghyeon Song, Two Higgs doublet models for the LHC Higgs boson data at $\sqrt{s} = 7$ and 8 TeV, J. High Energy Phys. 09 (2014) 101.

[25] Giacomo Cacciapaglia, Aldo Deandrea, Guillaume Drieu La Rochelle, and Jean-Baptiste Flament, Searching for a lighter Higgs boson: Parametrization and sample tests, Phys. Rev. D **91**, 015012 (2015).

[26] Jeremy Bernon, John F. Gunion, Yun Jiang, and Sabine Kraml, Light Higgs bosons in two-Higgs-doublet models, Phys. Rev. D **91**, 075019 (2015).

[27] Jérémy Bernon, John F. Gunion, Howard E. Haber, Yun Jiang, and Sabine Kraml, Scrutinizing the alignment limit in two-Higgs-doublet models. II, $m_H = 125$ GeV, Phys. Rev. D **93**, 035027 (2016).

[28] Giacomo Cacciapaglia, Aldo Deandrea, Suzanne Gascon-Shotkin, Solène Le Corre, Morgan Lethuillier, and Junquan Tao, Search for a lighter Higgs boson in two Higgs doublet models, J. High Energy Phys. 12 (2016) 068.

[29] Monoranjan Guchait, Aravind H. Vijay, and Jacky Kumar, Detection prospects of light pseudoscalar Higgs boson at the LHC, J. High Energy Phys. 08 (2017) 122.

[30] Disha Bhatia, Ushoshi Maitra, and Saurabh Niyogi, Discovery prospects of a light Higgs boson at the LHC in type-I 2HDM, Phys. Rev. D **97**, 055027 (2018).

[31] Ning Chen, Tong Li, Wei Su, and Yongcheng Wu, The future probe of the light Higgs boson pair production (2020).

[32] Alejandro Celis, Victor Ilisie, and Antonio Pich, LHC constraints on two-Higgs doublet models, J. High Energy Phys. 07 (2013) 053.

[33] Abdesslam Arhrib, Rachid Benbrik, Stefano Moretti, Abdessamad Rouchad, Qi-Shu Yan, and Xianhui Zhang, Multi-photon production in the type-I 2HDM, J. High Energy Phys. 07 (2018) 007.

[34] Benjamin Grinstein and Patipan Uttayarat, Carving out parameter space in type-II two Higgs doublets model, J. High Energy Phys. 06 (2013) 094; 09 (2013) 110(E).

[35] Chien-Yi Chen, S. Dawson, and Marc Sher, Heavy Higgs searches and constraints on two Higgs doublet models, Phys. Rev. D **88**, 015018 (2013); **88**, 039901(E) (2013).

[36] V. Khachatryan *et al.*, Search for light bosons in decays of the 125 GeV Higgs boson in proton-proton collisions at $\sqrt{s} = 8$ TeV, J. High Energy Phys. 10 (2017) 076.

[37] Albert M. Sirunyan *et al.*, Search for light pseudoscalar boson pairs produced from decays of the 125 GeV Higgs boson in final states with two muons and two nearby tracks in pp collisions at $\sqrt{s} = 13$ TeV, Phys. Lett. B **800**, 135087 (2020).

[38] Georges Aad *et al.*, Search for Higgs bosons decaying to aa in the $\mu\mu\tau\tau$ final state in pp collisions at $\sqrt{s} = 8$ TeV with the ATLAS experiment, Phys. Rev. D **92**, 052002 (2015).

[39] Albert M. Sirunyan *et al.*, Search for an exotic decay of the Higgs boson to a pair of light pseudoscalars in the final state of two muons and two τ leptons in proton-proton collisions at $\sqrt{s} = 13$ TeV, J. High Energy Phys. 11 (2018) 018.

[40] Albert M. Sirunyan *et al.*, Search for a light pseudoscalar Higgs boson in the boosted $\mu\mu\tau\tau$ final state in proton-proton collisions at $\sqrt{s} = 13$ TeV, J. High Energy Phys. 08 (2020) 139.

[41] Search for exotic decays of the Higgs boson to a pair of new light bosons in the $\mu\mu bb$ final state at $\sqrt{s} = 13$ TeV with the full run 2 dataset (2022).

[42] Search for exotic Higgs boson decays to a pair of pseudoscalars in the $\mu\mu$bb and $\tau\tau$bb final states in proton-proton collisions with the CMS experiment (2023).

[43] Albert M. Sirunyan *et al.*, Search for Higgs boson pair production in events with two bottom quarks and two tau leptons in proton–proton collisions at $\sqrt{s} = 13$ TeV, Phys. Lett. B **778**, 101 (2018).

[44] Albert M. Sirunyan *et al.*, Search for an exotic decay of the Higgs boson to a pair of light pseudoscalars in the final state with two b quarks and two τ leptons in proton-proton collisions at $\sqrt{s} = 13$ TeV, Phys. Lett. B **785**, 462 (2018).

[45] Morad Aaboud *et al.*, Search for Higgs boson decays to beyond-the-standard-model light bosons in four-lepton events with the ATLAS detector at $\sqrt{s} = 13$ TeV, J. High Energy Phys. 06 (2018) 166.

[46] Serguei Chatrchyan *et al.*, Search for a non-standard-model Higgs boson decaying to a pair of new light bosons in four-muon final states, Phys. Lett. B **726**, 564 (2013).

[47] V. Khachatryan *et al.*, A search for pair production of new light bosons decaying into muons, Phys. Lett. B **752**, 146 (2016).

[48] Albert M. Sirunyan *et al.*, A search for pair production of new light bosons decaying into muons in proton-proton collisions at 13 TeV, Phys. Lett. B **796**, 131 (2019).

[49] Georges Aad *et al.*, Search for Higgs bosons decaying into new spin-0 or spin-1 particles in four-lepton final states with the ATLAS detector with 139 fb^{-1} of pp collision data at $\sqrt{s} = 13$ TeV, J. High Energy Phys. 03 (2022) 041.

[50] F. Gianotti *et al.*, Physics potential and experimental challenges of the LHC luminosity upgrade, Eur. Phys. J. C **39**, 293 (2005).

[51] Abdesslam Arhrib, Rachid Benbrik, and Cheng-Wei Chiang, Probing triple Higgs couplings of the two Higgs doublet model at linear collider, Phys. Rev. D **77**, 115013 (2008).

[52] Shinya Kanemura, Mariko Kikuchi, and Kei Yagyu, Fingerprinting the extended Higgs sector using one-loop corrected Higgs boson couplings and future precision measurements, Nucl. Phys. **B896**, 80 (2015).

[53] Sheldon L. Glashow and Steven Weinberg, Natural conservation laws for neutral currents, Phys. Rev. D **15**, 1958 (1977).

[54] Shinya Kanemura, Takahiro Kubota, and Eiichi Takasugi, Lee-Quigg-Thacker bounds for Higgs boson masses in a two doublet model, Phys. Lett. B **313**, 155 (1993).

[55] Andrew G. Akeroyd, Abdesslam Arhrib, and El-Mokhtar Naimi, Note on tree level unitarity in the general two Higgs doublet model, Phys. Lett. B **490**, 119 (2000).

[56] Abdesslam Arhrib, Unitarity constraints on scalar parameters of the standard and two Higgs doublets model, in *Proceedings of the Workshop on Noncommutative Geometry, Superstrings and Particle Physics* (2000).

[57] Nilendra G. Deshpande and Ernest Ma, Pattern of symmetry breaking with two Higgs doublets, Phys. Rev. D **18**, 2574 (1978).

[58] David Eriksson, Johan Rathsman, and Oscar Stal, 2HDMC: Two-Higgs-doublet model calculator physics and manual, Comput. Phys. Commun. **181**, 189 (2010).

[59] Philip Bechtle, Daniel Dercks, Sven Heinemeyer, Tobias Klingl, Tim Stefaniak, Georg Weiglein, and Jonas Wittbrodt, HiggsBounds-5: Testing Higgs sectors in the LHC 13 TeV era, Eur. Phys. J. C **80**, 1211 (2020).

[60] Philip Bechtle, Sven Heinemeyer, Tobias Klingl, Tim Stefaniak, Georg Weiglein, and Jonas Wittbrodt, HiggsSignals-2: Probing new physics with precision Higgs measurements in the LHC 13 TeV era, Eur. Phys. J. C **81**, 145 (2021).

[61] Hong-Jian He, Nir Polonsky, and Shu-fang Su, Extra families, Higgs spectrum and oblique corrections, Phys. Rev. D **64**, 053004 (2001).

[62] W. Grimus, L. Lavoura, O. M. Ogreid, and P. Osland, The oblique parameters in multi-Higgs-doublet models, Nucl. Phys. **B801**, 81 (2008).

[63] Howard E. Haber and Deva O'Neil, Basis-independent methods for the two-Higgs-doublet model III: The *CP*-conserving limit, custodial symmetry, and the oblique parameters S, T, U, Phys. Rev. D **83**, 055017 (2011).

[64] P. A. Zyla *et al.*, Review of particle physics, Prog. Theor. Exp. Phys. **2020**, 083C01 (2020).

[65] F. Mahmoudi, SuperIso v2.3: A program for calculating flavor physics observables in supersymmetry, Comput. Phys. Commun. **180**, 1579 (2009).

[66] Yasmine Sara Amhis *et al.*, Averages of b-hadron, c-hadron, and τ-lepton properties as of 2021, Phys. Rev. D **107**, 052008 (2023).

[67] Roel Aaij *et al.*, Measurement of the $B_s^0 \to \mu^+\mu^-$ decay properties and search for the $B^0 \to \mu^+\mu^-$ and $B_s^0 \to \mu^+\mu^-\gamma$ decays, Phys. Rev. D **105**, 012010 (2022).

[68] R. Aaij *et al.*, Analysis of neutral B-meson decays into two muons, Phys. Rev. Lett. **128**, 041801 (2022).

[69] Armen Tumasyan *et al.*, Measurement of the $B_S^0 \to \mu^+\mu^-$ decay properties and search for the $B^0 \to \mu^+\mu^-$ decay in proton-proton collisions at $\sqrt{s} = 13$ TeV, Phys. Lett. B **842**, 137955 (2023).

[70] M. Misiak, Abdur Rehman, and Matthias Steinhauser, Towards $\bar{B} \to X_s\gamma$ at the NNLO in QCD without interpolation in m_c, J. High Energy Phys. 06 (2020) 175.

[71] Mikolaj Misiak and Matthias Steinhauser, Weak radiative decays of the B meson and bounds on $M_{H^\pm}$ in the two-Higgs-doublet model, Eur. Phys. J. C **77**, 201 (2017).

[72] Johannes Haller, Andreas Hoecker, Roman Kogler, Klaus Mönig, Thomas Peiffer, and Jörg Stelzer, Update of the global electroweak fit and constraints on two-Higgs-doublet models, Eur. Phys. J. C **78**, 675 (2018).

[73] Georges Aad *et al.*, Search for charged Higgs bosons through the violation of lepton universality in $t\bar{t}$ events using pp collision data at $\sqrt{s} = 7$ TeV with the ATLAS experiment, J. High Energy Phys. 03 (2013) 076.

[74] Georges Aad *et al.*, Search for charged Higgs bosons decaying via $H^+ \to \tau\nu$ in top quark pair events using pp collision data at $\sqrt{s} = 7$ TeV with the ATLAS detector, J. High Energy Phys. 06 (2012) 039.

[75] Serguei Chatrchyan *et al.*, Search for a light charged Higgs boson in top quark decays in pp collisions at $\sqrt{s} = 7$ TeV, J. High Energy Phys. 07 (2012) 143.

[76] Georges Aad *et al.*, Search for charged Higgs bosons decaying via $H^\pm \to \tau^\pm\nu$ in fully hadronic final states using pp collision data at $\sqrt{s} = 8$ TeV with the ATLAS detector, J. High Energy Phys. 03 (2015) 088.

[77] Vardan Khachatryan *et al.*, Search for a charged Higgs boson in pp collisions at $\sqrt{s} = 8$ TeV, J. High Energy Phys. 11 (2015) 018.

[78] Morad Aaboud *et al.*, Search for charged Higgs bosons decaying via $H^\pm \to \tau^\pm\nu_\tau$ in the $\tau +$ jets and $\tau +$ lepton final states with 36 fb^{-1} of pp collision data recorded at $\sqrt{s} = 13$ TeV with the ATLAS experiment, J. High Energy Phys. 09 (2018) 139.

[79] Albert M. Sirunyan *et al.*, Search for charged Higgs bosons in the $H^\pm \to \tau^\pm\nu_\tau$ decay channel in proton-proton collisions at $\sqrt{s} = 13$ TeV, J. High Energy Phys. 07 (2019) 142.

[80] Georges Aad *et al.*, Search for a light charged Higgs boson in the decay channel $H^+ \to c\bar{s}$ in $t\bar{t}$ events using pp collisions at $\sqrt{s} = 7$ TeV with the ATLAS detector, Eur. Phys. J. C **73**, 2465 (2013).

[81] Vardan Khachatryan *et al.*, Search for a light charged Higgs boson decaying to $c\bar{s}$ in pp collisions at $\sqrt{s} = 8$ TeV, J. High Energy Phys. 12 (2015) 178.

[82] Albert M. Sirunyan *et al.*, Search for a light charged Higgs boson in the $H^\pm \to cs$ channel in proton-proton collisions at $\sqrt{s} = 13$ TeV, Phys. Rev. D **102**, 072001 (2020).

[83] Albert M. Sirunyan *et al.*, Search for a charged Higgs boson decaying to charm and bottom quarks in proton-proton collisions at $\sqrt{s} = 8$ TeV, J. High Energy Phys. 11 (2018) 115.

[84] Albert M. Sirunyan *et al.*, Search for a light charged Higgs boson decaying to a W boson and a *CP*-odd Higgs boson in final states with e$\mu\mu$ or $\mu\mu\mu$ in proton-proton collisions at $\sqrt{s} = 13$ TeV, Phys. Rev. Lett. **123**, 131802 (2019).

[85] G. Aad *et al.*, Search for a light charged Higgs boson in $t \to H^\pm b$ decays, with $H^\pm \to cb$, in the lepton + jets final state in proton-proton collisions at $\sqrt{s} = 13$ TeV with the ATLAS detector, J. High Energy Phys. 09 (2023) 004.

[86] F. Arco, S. Heinemeyer, and M. J. Herrero, Exploring sizable triple Higgs couplings in the 2HDM, Eur. Phys. J. C **80**, 884 (2020).

[87] A. G. Akeroyd, Three body decays of Higgs bosons at LEP-2 and application to a hidden fermiophobic Higgs, Nucl. Phys. **B544**, 557 (1999).

[88] Abdesslam Arhrib, Rachid Benbrik, and Stefano Moretti, Bosonic decays of charged Higgs bosons in a 2HDM type-I, Eur. Phys. J. C **77**, 621 (2017).

[89] A. Arhrib, R. Benbrik, M. Krab, B. Manaut, S. Moretti, Yan Wang, and Qi-Shu Yan, New discovery modes for a light charged Higgs boson at the LHC, J. High Energy Phys. 10 (2021) 073.

[90] Georges Aad *et al.*, Evidence of off-shell Higgs boson production from ZZ leptonic decay channels and constraints on its total width with the ATLAS detector (2023).

[91] Armen Tumasyan *et al.*, Measurement of the Higgs boson width and evidence of its off-shell contributions to ZZ production, Nat. Phys. **18**, 1329 (2022).

[92] Robert V. Harlander, Stefan Liebler, and Hendrik Mantler, SusHi: A program for the calculation of Higgs production in gluon fusion and bottom-quark annihilation in the standard model and the MSSM, Comput. Phys. Commun. **184**, 1605 (2013).

[93] Robert V. Harlander, Stefan Liebler, and Hendrik Mantler, SusHi Bento: Beyond NNLO and the heavy-top limit, Comput. Phys. Commun. **212**, 239 (2017).

[94] Robert V. Harlander and William B. Kilgore, Next-to-next-to-leading order Higgs production at hadron colliders, Phys. Rev. Lett. **88**, 201801 (2002).

[95] Charalampos Anastasiou, Claude Duhr, Falko Dulat, Franz Herzog, and Bernhard Mistlberger, Higgs boson gluon-fusion production in QCD at three loops, Phys. Rev. Lett. **114**, 212001 (2015).

[96] M. Cepeda *et al.*, Report from working group 2: Higgs physics at the HL-LHC and HE-LHC, CERN Yellow Rep. Monogr. **7**, 221 (2019).

[97] S. Moretti, S. Semlali, and C. H. Shepherd-Themistocleous (The ATLAS Collaboration), Combination of searches for invisible decays of the Higgs boson using 139 fb − 1 of proton-proton collision data at $s = 13$ TeV collected with the ATLAS experiment, Phys. Lett. B **842**, 137963 (2023).

[98] A search for decays of the Higgs boson to invisible particles in events with a top-antitop quark pair or a vector boson in proton-proton collisions at $\sqrt{s} = 13$ TeV (2023).

[99] Search for exotic decay of the Higgs boson into two light pseudoscalars with four photons in the final state at $\sqrt{s} =$ 13 TeV (2021).

[100] Georges Aad *et al.*, Search for Higgs boson decays into a pair of pseudoscalar particles in the $bb\mu\mu$ final state with the ATLAS detector in pp collisions at $\sqrt{s} = 13$ TeV, Phys. Rev. D **105**, 012006 (2022).

[101] S. Moretti, S. Semlali, and C. H. Shepherd-Themistocleous, A novel experimental search channel for very light Higgses in the 2HDM type I (2022).

[102] Peter Uwer, EasyNData: A simple tool to extract numerical values from published plots (2007).

[103] Rikard Enberg, William Klemm, Stefano Moretti, and Shoaib Munir, Electroweak production of light scalar–pseudoscalar pairs from extended Higgs sectors, Phys. Lett. B **764**, 121 (2017).

[104] S. Schael *et al.*, Search for neutral MSSM Higgs bosons at LEP, Eur. Phys. J. C **47**, 547 (2006).

[105] S. Schael *et al.*, Precision electroweak measurements on the Z resonance, Phys. Rep. **427**, 257 (2006).

[106] Patrick Janot and Stanisław Jadach, Improved Bhabha cross section at LEP and the number of light neutrino species, Phys. Lett. B **803**, 135319 (2020).

[107] Georges Aad *et al.*, Search for new phenomena in events with at least three photons collected in pp collisions at $\sqrt{s} = 8$ TeV with the ATLAS detector, Eur. Phys. J. C **76**, 210 (2016).

[108] Albert M. Sirunyan *et al.*, Search for an exotic decay of the Higgs boson to a pair of light pseudoscalars in the final state with two muons and two b quarks in pp collisions at 13 TeV, Phys. Lett. B **795**, 398 (2019).

[109] Kaoru Hagiwara, Tong Li, Kentarou Mawatari, and Junya Nakamura, TauDecay: A library to simulate polarized tau decays via FeynRules and MadGraph5, Eur. Phys. J. C **73**, 2489 (2013).

[110] J. Alwall, R. Frederix, S. Frixione, V. Hirschi, F. Maltoni, O. Mattelaer, H. S. Shao, T. Stelzer, P. Torrielli, and M. Zaro, The automated computation of tree-level and next-to-leading order differential cross sections, and their matching to parton shower simulations, J. High Energy Phys. 07 (2014) 079.

[111] Fernando Febres Cordero, L. Reina, and D. Wackeroth, W- and Z-boson production with a massive bottom-quark pair at the Large Hadron Collider, Phys. Rev. D **80**, 034015 (2009).

[112] T. Binoth *et al.*, The SM and NLO multileg working group: Summary report, in *Proceedings of the 6th Les Houches Workshop on Physics at TeV Colliders* (2010), pp. 21–189.

[113] Torbjorn Sjostrand, Stephen Mrenna, and Peter Z. Skands, PYTHIA 6.4 physics and manual, J. High Energy Phys. 05 (2006) 026.

[114] J. de Favereau, C. Delaere, P. Demin, A. Giammanco, V. Lemaître, A. Mertens, and M. Selvaggi, DELPHES 3, A modular framework for fast simulation of a generic collider experiment, J. High Energy Phys. 02 (2014) 057.

[115] Eric Conte, Benjamin Fuks, and Guillaume Serret, MadAnalysis 5, A user-friendly framework for collider phenomenology, Comput. Phys. Commun. **184**, 222 (2013).

[116] Vardan Khachatryan *et al.*, The CMS trigger system, J. Instrum. **12**, P01020 (2017).

[117] A. M. Sirunyan *et al.*, Performance of reconstruction and identification of τ leptons decaying to hadrons and ν_τ in pp collisions at $\sqrt{s} = 13$ TeV, J. Instrum. **13**, P10005 (2018).

[118] Swagata Mukherjee, Data scouting and data parking with the CMS high level trigger, Proc. Sci. EPS-HEP2019 (**2020**) 139.

[119] Robert Bainbridge, Recording and reconstructing 10 billion unbiased b hadron decays in CMS, EPJ Web Conf. **245**, 01025 (2020).

[120] Matteo Cacciari, Gavin P. Salam, and Gregory Soyez, The anti-k_t jet clustering algorithm, J. High Energy Phys. 04 (2008) 063.

[121] Yuri L. Dokshitzer, G. D. Leder, S. Moretti, and B. R. Webber, Better jet clustering algorithms, J. High Energy Phys. 08 (1997) 001.

[122] M. Wobisch and T. Wengler, Hadronization corrections to jet cross sections in deep inelastic scattering, in *Proceedings of the Workshop on Monte Carlo Generators for HERA Physics (Plenary Starting Meeting)* (1998), pp. 270–279.

[123] CMS Collaboration, Identification of b-quark jets with the CMS experiment, J. Instrum. **8**, P04013 (2013).

[124] A. M. Sirunyan *et al.*, Identification of heavy-flavour jets with the CMS detector in pp collisions at 13 TeV, J. Instrum. **13**, P05011 (2018).

[125] Antimo Cagnotta, Francesco Carnevali, and Agostino De Iorio, Machine learning applications for jet tagging in the CMS experiment, Appl. Sci. **12**, 10574 (2022).